ELASTIC/PLASTIC BEHAVIOR OF CHALCOGENIDE GLASSES IN THE Ge-Sb-Se SYSTEM

BY

BADRI RANGARAJAN

A THESIS
SUBMITTED TO THE FACULTY OF

ALFRED UNIVERSITY

IN PARTIAL FULFILLMENT OF THE REQUIREMENTS
FOR THE DEGREE OF

MASTER OF SCIENCE

IN

CERAMIC ENGINEERING

ALFRED, NEW YORK

APRIL, 2004

ELASTIC/PLASTIC BEHAVIOR OF CHALCOGENIDE GLASSES IN THE Ge-Sb-Se SYSTEM

BY

BADRI RANGARAJAN

B.TECH. ANNA UNIVERSITY, INDIA (2002)

SIGNATURE OF AUTHOR (Signature on file)

APPROVED BY (Signature on file)
ARUN VARSHNEYA, ADVISOR

(Signature on file)
WILLIAM LaCOURSE, ADVISORY COMMITTEE

(Signature on file)
ALEXIS CLARE, ADVISORY COMMITTEE

(Signature on file)
DOREEN EDWARDS, CHAIR, ORAL THESIS DEFENSE

ACCEPTED BY (Signature on file)
ALASTAIR CORMACK, DEAN,
SCHOOL OF ENGINEERING

ACKNOWLEDGMENTS

Words cannot express my gratitude to my advisor Dr. Arun K. Varshneya, for his assistance and guidance throughout the course of this thesis. Had he not concerned about me in getting my work done, this masters thesis would have been impossible in such quick time.

I wish to thank Dr. Alexander Fluegel for his innumerable assistance with the computer.

My sincere thanks to Dr. Steven J. Mayes; Dr. Franz Magerl, Fachhochschule Amberg-Weiden, Germany; and Mr. Todd S. Nichols, Machine Systems Analyst, STI Technologies Inc., Rochester, NY for their assistance with finite element analysis computations.

I would like to thank fellow graduate students, Mr. Sreekumar Chockalingam, Amit Shah Rajnikant and V.C. Ram Mohan for their help and encouragement.

Finally, I express my deep sense of gratitude to my parents for their support and love and to my brother for providing me with the finest education.

TABLE OF CONTENTS

LIST OF TABLES

LIST OF FIGURES

ABSTRACT

Elastic/plastic behavior of chalcogenide glasses in the Ge-Se and Ge-Sb-Se systems was studied using different spherical indenters: 400μm and 2mm. Static room temperature indentations were carried out to determine the trends in hardness, fracture toughness and brittleness with respect to the average covalent coordination number, <r>. Binary glasses show maximization in fracture toughness and minimization in brittleness at the composition $Ge_{20}Se_{80}$. No such trends were observed for ternary glasses. Indentations were also performed at -80°C to ensure that the trends are due to structural considerations of optimized connectivity. LBH and elastic modulus increase linearly with the network connectivity. Elastically recovered energy increases with indenter diameter showing a local maximum at $Ge_{20}Se_{80}$. Finite element simulations of binary glasses also show similar trends for LBH and DBH. Increasing elastic moduli cause stresses to increase with <r> for a given indenter ball diameter. Computed yield stresses, when plotted against <r>, show small deviations from apparent linearity at <r> = 2.4, giving another hand to the theory of rigidity percolation.

1 INTRODUCTION

Chalcogenide glasses are formed by melting one or more of the chalcogen elements (S, Se, Te) with more electropositive elements such as As and Ge, P, Sb, Bi, Si, Sn, Pb, B, Al, Ga, In, Tl, Ag, lanthanides and Na.[1] Some of these glass compositions are unique in the sense that they can transmit light in the second atmospheric window, from 8 to 14μm.[2] This makes them potentially available in fiber-form for applications such as IR sensors, CO_2 laser-assisted microsurgery and optical amplifiers. They have bandgap energies of 1-3eV and behave as amorphous semiconductors. They bear some similarity to oxide glasses but there is a marked difference caused by the nature of atomic bonding.[3]

The chemical bonding of the matrix is directional and covalent. The atomic average covalent coordination number, <r>, obeys the Mott's 8 – N rule, where N is the atom's valency, and describes the crosslinking between these atoms. Additionally, heteropolar bonds would be favored over homopolar bonds, as is given by the Chemically Ordered Covalent Network Model (COCN).[4] In general, the bonds formed between the individual atoms in these glasses are more rigid than that of in organic polymers and more flexible than that of in oxide glasses. Accordingly, the glass transition temperatures and elastic properties lie in between those of these materials.

1.1 PERCOLATION PROCESS

In 1979, Phillips put forth his constraints hypothesis.[5] The gist of his argument is that there exists a rigidity percolation threshold at <r> = 2.45, where the number of degrees of freedom just exhausts the number of constraints imposed by bond bending and bond stretching forces. This is later modified by Dohler et al. as <r> = 2.4.[6] This match also minimizes both the strain energy of the network[7] and the configurational entropy. He commented that there would be ideal glass formation at <r> = 2.4, because glasses of that particular coordination number undergo the least number of configurational rearrangements in transforming to a glass. His theory is also called as the Valence Force Field Theory.

Phillips and Thorpe, in 1985, expanded the theory of rigidity percolation.[8] Thorpe suggested that below <r> = 2.4, the glass network is composed of floppy or zero-frequency vibrational modes and is unbraced or underconstrained.[9] The converse is true above 2.4, where the glass is overbraced or overconstrained. When <r> reaches the value of 2.4, the number of zero-frequency modes should diminish to zero and there should be optimum network connectivity. This is shown in Figure 1.1. His conclusion is that all mechanical properties should maximize at <r> = 2.4.

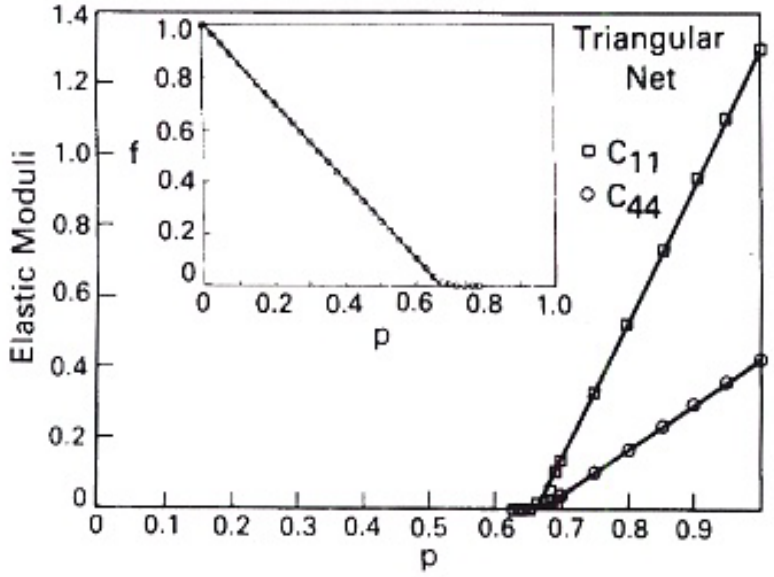

Figure 1.1. The elastic moduli versus percolation probability for a 440 atom triangular network. The insert shows fraction of zero frequency modes for a 168 atom triangular network. (From Thorpe[9])

Tanaka, in 1988, analyzed medium-range structural orders in chalcogenide glasses.[10] He showed that there exists a structural phase transition at <r> = 2.67 in addition to that at 2.4 predicted by Phillips and others. He studied the physical properties (shown in Figure 1.2) as a function of the coordination number and concluded that glasses with <r> ≤ 2.67, may have low-dimensional structures, in which the intermolecular force governs the physical properties. In contrast, covalent glasses of <r> > 2.67 seem to be cross-linked three dimensionally. So, there are two kinds of topological thresholds observed in chalcogenide glasses when their properties are studied

as a function of coordination number. One is at <r> = 2.4, the physical threshold, and the other is at <r> = 2.67, the chemical threshold.

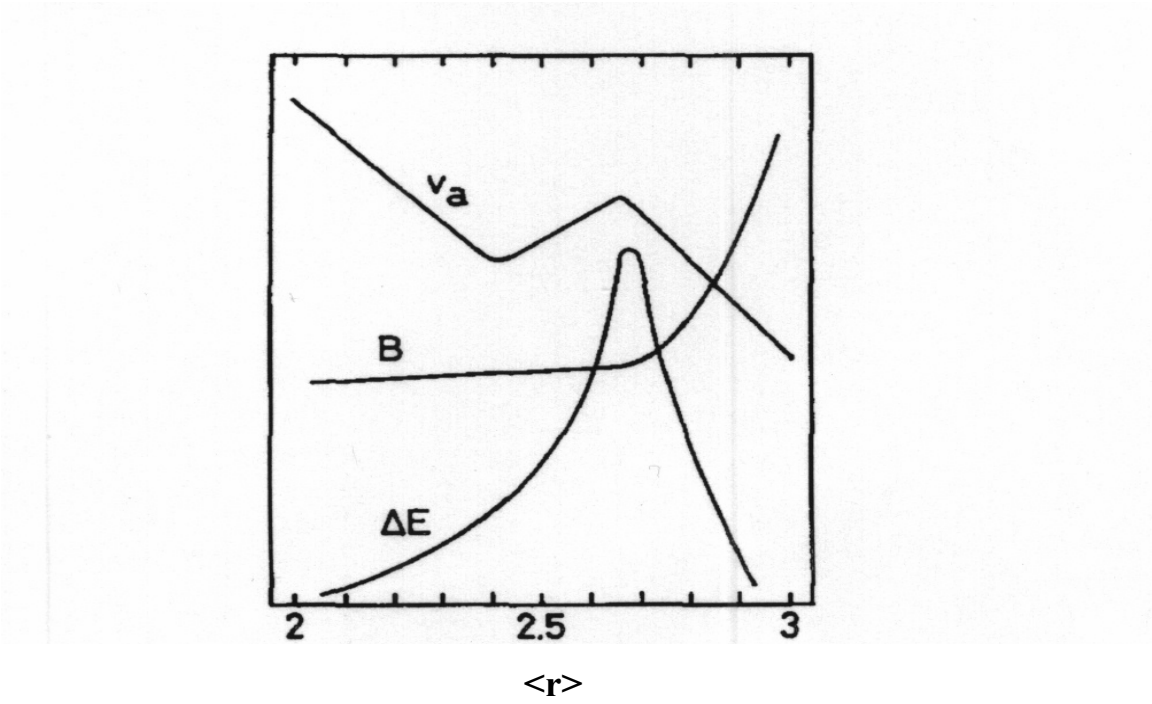

Figure 1.2. Qualitative features of the atomic volume v_a, the bulk modulus B and the magnitude of the reversible photodarkening ΔE as a function of the average coordination number <r>. (From Tanaka[10])

1.2 SUMMARY OF FINDINGS SO FAR

Varshneya and others, in 1990, studied the various physical properties as a function of <r> to find extrema near <r> = 2.4/2.67.[11] Two of their significant findings are that the Vickers Hardness Number (VHN) and the glass transition temperature (T_g), both increased with the connectivity of the network.[12,13] A linear equation is fit to the hardness data and a modified Gibbs-DiMarzio equation is fit to T_g data. The results are shown in Figure 1.3 and Figure 1.4. None of the properties showed extrema at the topological thresholds except the molar volume, which showed a minimum.[14] Their results are summarized in Table 1.

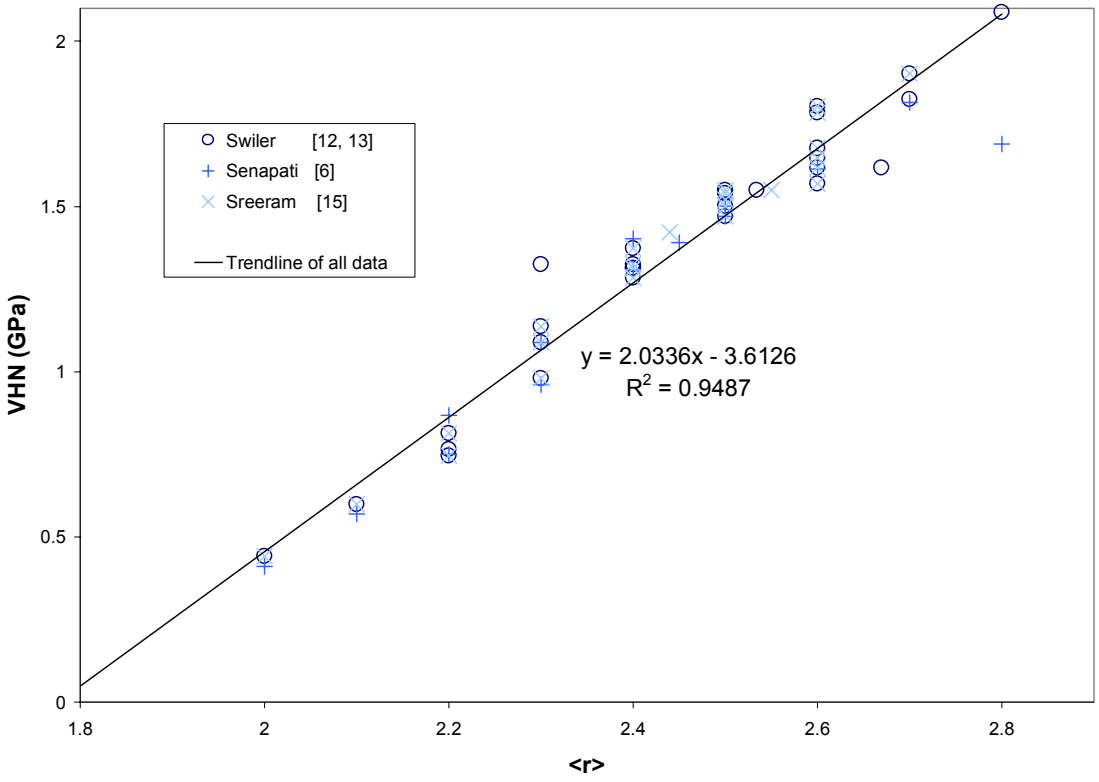

Figure 1.3. VHN as a function of the average coordination number for Ge-Se and Ge-Sb-Se systems from static hardness measurements. A linear trend is observed. (From Firstenberg[15])

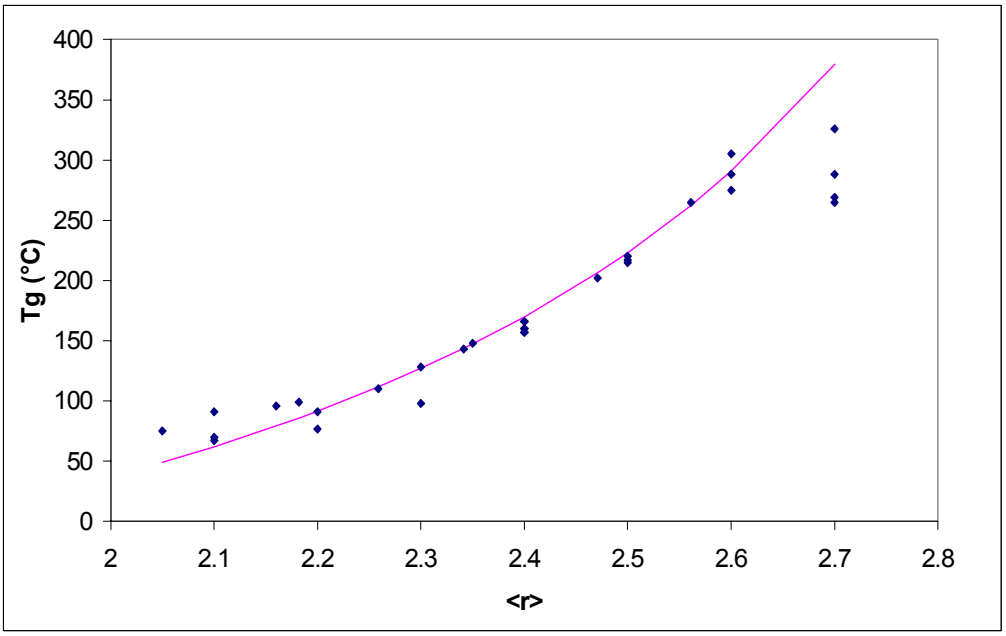

Figure 1.4. Glass transition temperature (T_g), determined from DSC measurements, plotted versus the average coordination number. A modified Gibbs-DiMarzio equation is fit to the data. (From Strange[16])

Table I. Property Trends vs <r> for Glasses in the Ge-Sb-Se System.*

Property	<r> = 2.0 to 2.4	<r> = 2.4	<r> = 2.4 to tie line	Tie line	Past tie line
Molar Volume	Decreases	Minimum	Increases	Maxima	Decreases
Poisson's ratio	Decreases	----------	----------→	Local minimum	Local maximum
Elastic Moduli	Generally increase	Some (?) steepening	Generally increase	Shallow local extrema	Generally increase
Vickers Hardness	Increases	----------	----------→	Shallow local extrema	Increases
Indentation Toughness	Increases	----------	----------→	Maxima	Decreases
Glass Transition Temperature	Increases	----------	----------→	Maxima	Decreases

*(From Strange,[16] which is in itself adapted from Varshneya and others[11])

Senapati et al. studied the thermodynamic properties, specific heat capacity (C_p), coefficient of thermal expansion (α) and isothermal compressibility (κ_T), as a function of the coordination number <r> and observed a minimum in ΔC_p and $\Delta\alpha$ during the glass transition as well as in the supercooled liquid state.[17] Since the increase in heat capacity at around T_g is due to the associated configurational changes, he concluded that the glasses of the coordination number 2.4 undergo the minimum configurational changes or the least structural relaxation on annealing.[18,19] "Least structural relaxation" means that the coordination number, <r> = 2.4, forms the "strongest glass" as classified by C. A. Angell.[20,21,22] Also, recent publications by Boolchand et al. suggest that <r> = 2.4 glasses are thermally reversible due to structural self-organization of disordered networks.[23,24]

Since no significant physical property showed extrema at <r> = 2.4 in the glassy state, later investigators focused their research on the elastic/plastic behavior of chalcogenide glasses.

1.3 OBSERVATIONS MADE BY FIRSTENBERG, STRANGE AND BOWDEN

Since dynamic micro-hardness measurements are more sensitive to structural changes rather than static hardness measurements, Firstenberg used a recording micro-indenter to study the mechanical behavior of glasses.[15] He observed the Dynamic Vickers Hardness (DVH), which is calculated from the final penetration depth, and the elastic energy (E_e), which is the area under the unloading curve, to show maxima at around <r> = 2.4 for the binary system. However, the VHN, calculated assuming that the indentation retains the shape of the indenter after removal of load, did not show any maximum at <r> = 2.4, as we have already seen in Figure 1.3. So, Firstenberg pointed out that the indenter shape is not retained during unloading and has a higher preferential elastic recovery in the z-direction when compared to x- and y-directions as shown in Figure 1.5.

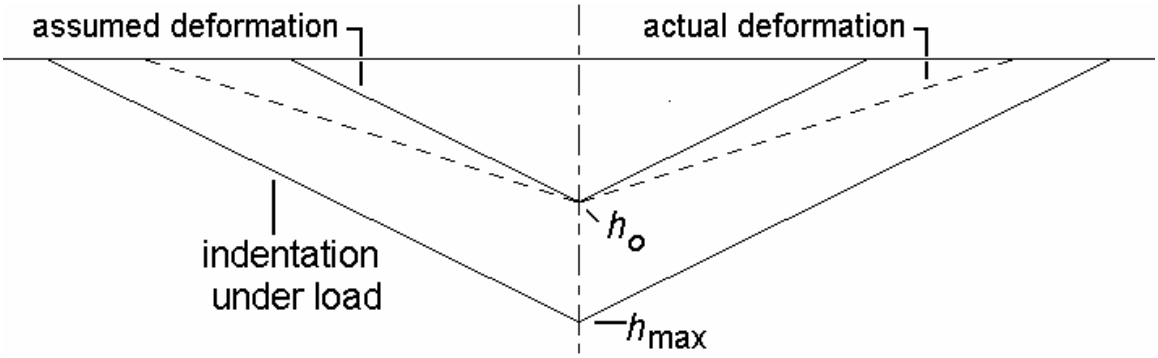

Figure 1.5. Unloading behavior of the sample during recording micro-hardness test. (From Firstenberg[15])

The higher recovery of <r> = 2.4 glasses in the z-direction causes them to have a lower final penetration depth and this explains the trends observed in DVH and E_e. Firstenberg attributed the high elastic recovery of <r> = 2.4 glasses to their high plastic yield strength values. He also modeled a basic stress-strain diagram based on the assumption of ideal elasticity-plasticity. The graph is shown in Figure 1.6. This is of great significance since it relates all the observed trends to a basic material property, the yield stress.

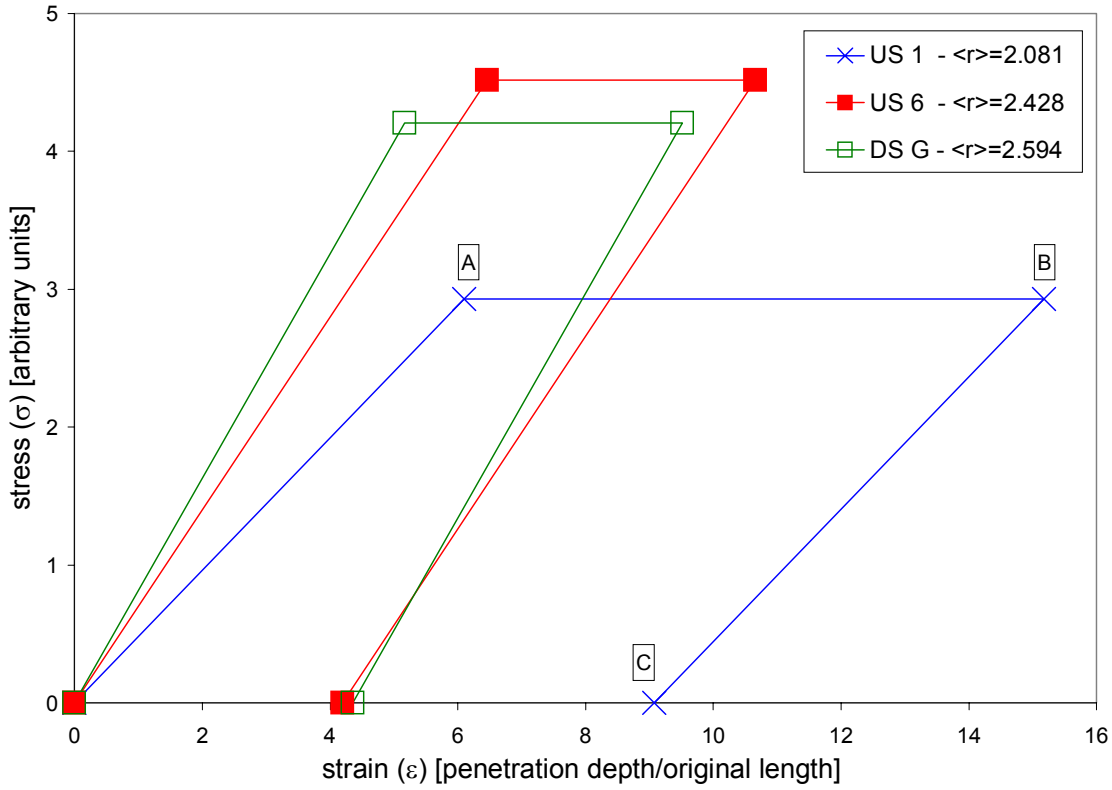

Figure 1.6. Stress-strain curve assuming ideal elasticity-plasticity for three glasses in the Ge-Se binary system. (From Firstenberg[15])

Strange was originally focused on the elastic threshold behavior of chalcogenide glasses.[16] He continued his dynamic hardness measurements using the same Vickers indenter but was troubled by the observations that the samples exhibited radial cracks around indentation corners even at loads as low as 50g. This provoked him to characterize the cracking behavior. He observed the brittleness, defined as the ratio of hardness to fracture toughness, to decrease and reach a minimum at <r> = 2.4 for the binary system, as shown in Figure 1.7. He assumed that the recoverable elastic energy would have been lost in the cracking of the more brittle glass and correlated it to the DVH and E_e trends observed by Firstenberg.

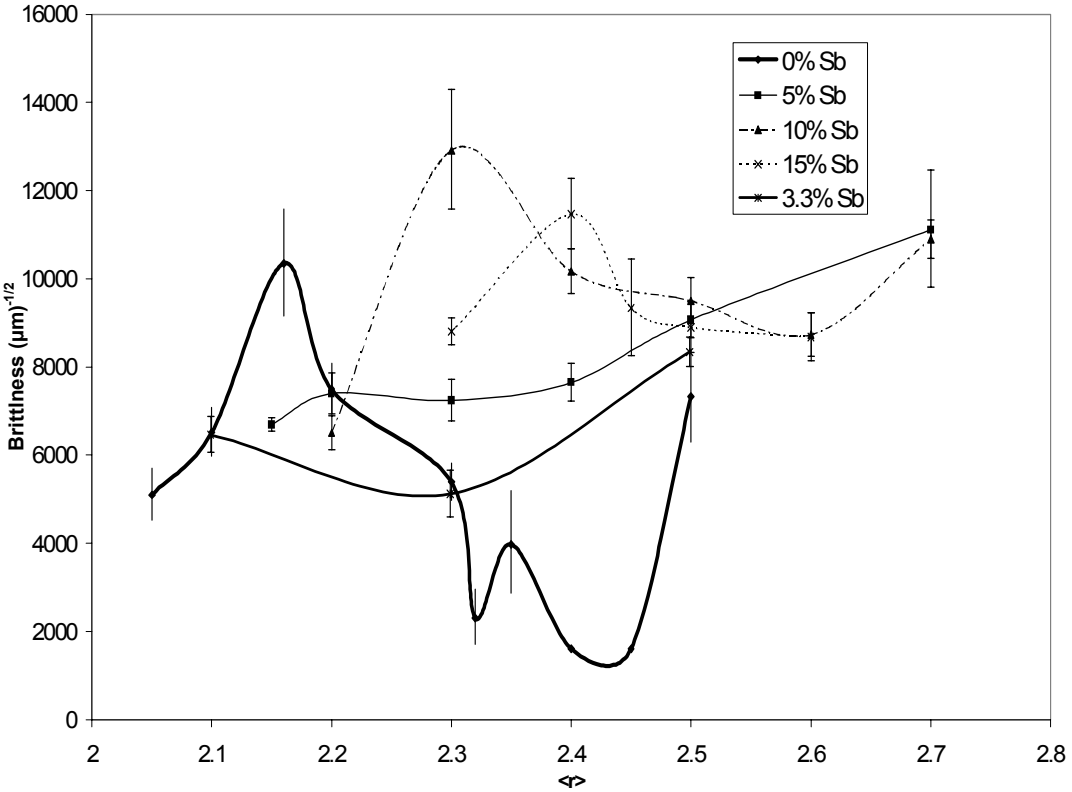

Figure 1.7. Brittleness vs <r> for glasses in Ge-Se and Ge-Sb-Se systems with data broken up into curves of equal Sb content. Minimization in brittleness occurs in the binary system at <r> = 2.4. (From Strange[16])

A square pyramid indenter magnifies the stresses around indentation corners and hence radial cracks are observed. Also, it creates a higher plastic deformation at very small loads, which makes the calculation of yield point extremely difficult. Bowden, in a recent Bachelor's thesis, carried out dynamic micro-hardness measurements using a 1mm diameter spherical (also called Hertzian or Brinell) indenter, in an attempt to explain the property maxima observed in chalcogenide glasses.[25] He observed the shape of indentations using a Zygo interferometer. No cracking was observed, but plastic "pileup" was evident around the circumference of indentation, as shown in Figure 1.8. The strain values observed using a 1mm ball indenter are low when compared to a Vickers indenter. So, in order to have high strain values, which, in turn, would maximize all the observed effects, an indenter of lower diameter should be chosen.

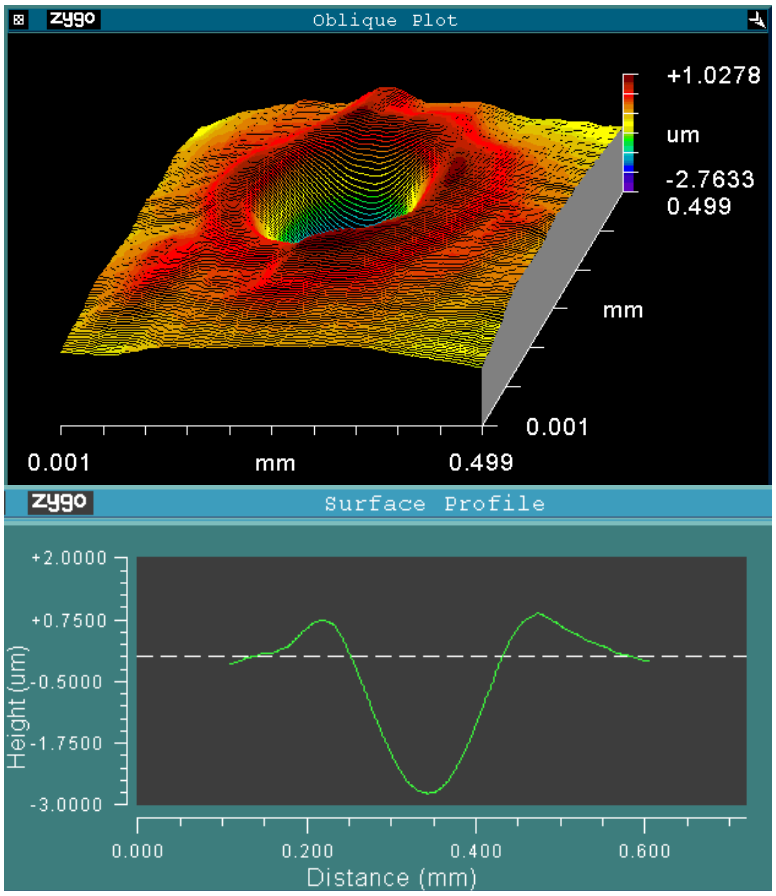

Figure 1.8. Laser interferometer trace of an indentation on selenium glass formed under a 1375g load using a 1mm diameter spherical indenter (top). A cross section of the indentation is shown at the bottom. (From Bowden[25])

1.4 OBJECTIVE OF THE PRESENT STUDY

The objective of this study is to carry out dynamic and static micro-hardness measurements to confirm the results obtained by prior investigators. Two spherical indenters are used for dynamic analysis; one is of 400μm diameter and the other 2mm. Brittleness and fracture toughness calculations were performed using static indentation measurements to confirm the results obtained by Strange. Finally, a finite element analysis of the glass, assuming elasticity-plasticity, was done to simulate the dynamic indentation behavior. The computed results are then compared with the experimental data in order to calculate the yield stress of glass with respect to the coordination number.

1.5 GLASS SAMPLES USED FOR THE ANALYSIS

The procedures for fabricating chalcogenide glasses from raw materials are given elsewhere.[26] Numerous glass samples, labeled in reference to the individuals who made

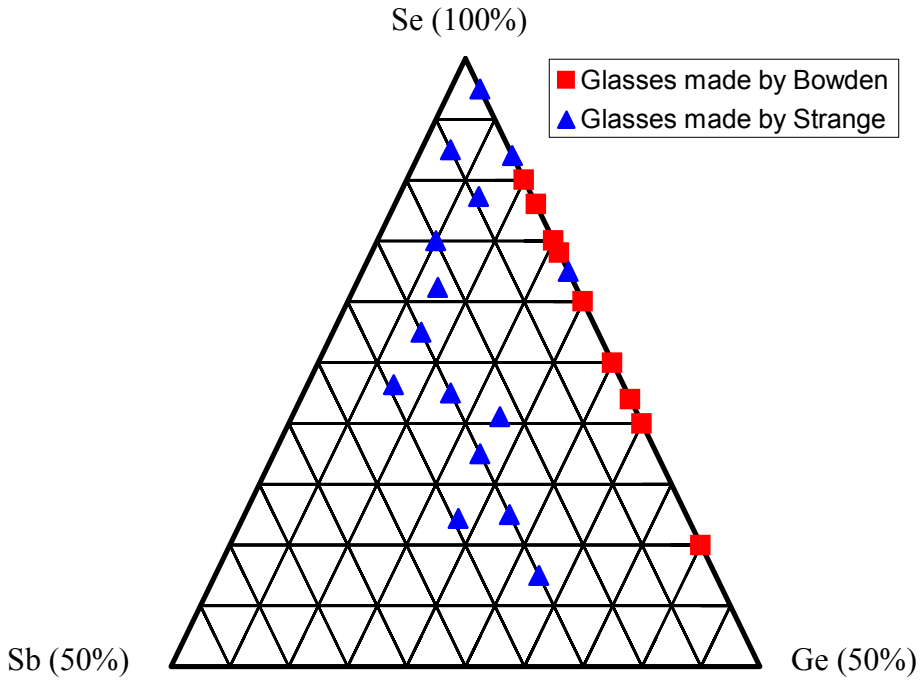

Figure 1.9. Ge-Sb-Se phase diagram indicating the glass compositions used for the analysis. Glasses made by two prior investigators are separately indicated.

it, were available and stored in airtight containers. Among them, the binary and ternary samples used for this study were selected from a list of glasses melted by two recent prior investigators, Strange and Bowden, who worked on the system of interest (Ge-Sb-Se). Samples, which were in good condition, were chosen in such a way that they cover the entire spectrum of average coordination numbers, from <r> = 2.0 to <r> = 2.8. The glass compositions used for the study are summarized in Table 2 and their locations in the phase diagram are shown in Figure 1.9.

Table II. Binary and Ternary Chalcogenide Glass Compositions Used for the Analysis

<r>	Ge (mol%)	Sb (mol%)	Se (mol%)
2.05	2.5	0	97.5
2.1	2.5	5	92.5
2.16	8	0	92
2.18	6.82	4.55	88.63
2.2	5	10	85
2.2	10	0	90
2.24	12	0	88
2.26	7.06	11.77	81.17
2.3	15	0	85
2.3	7.5	15	77.5
2.32	16	0	84
2.34	7.32	19.51	73.16
2.35	17.5	0	82.5
2.4	20	0	80
2.4	12.5	15	72.5
2.47	17.65	11.77	70.58
2.5	25	0	75
2.5	17.5	15	67.5
2.56	28	0	72
2.56	18.3	19.51	62.19
2.6	30	0	70
2.6	22.5	15	62.5
2.7	40	0	60
2.8	27.5	15	57.5

Disc-shaped samples were used for both static and dynamic hardness measurements. The samples were already ground flat with 600 and 1000 SiC grits and well polished with 0.3μm alumina powder with surfaces parallel to within 2°. The diameter and thickness of the samples ranged approximately from 8-15mm and 2-6mm respectively.

2 DYNAMIC MICRO INDENTATION MEASUREMENTS

2.1 BRINELL HARDNESS NUMBER

The hardness measured by indenting a smooth surface with a rigid sphere is called Brinell hardness. The Brinell Hardness Number (BHN), expressed as the ratio of the load P to the curved area of the indentation, is given by,

$$\text{BHN (kg/mm}^2\text{)} = \frac{2P}{[\pi D(D-\sqrt{(D^2-d^2)})]} \tag{2.1}$$

where P is the load in kg, D is the diameter of the ball in mm and d is the chordal diameter of the indentation in mm. In dynamic indentation measurements, in which the load is continuously recorded as a function of penetration depth, different Brinell hardness values such as Loaded Brinell Hardness (LBH) and Dynamic Brinell Hardness (DBH) can be calculated based on the penetration depth as will be seen a little later.

2.2 EXPERIMENTAL PROCEDURE

Micro-hardness measurements were made using the load and depth sensing dynamic micro-indenter (shown in Figure 2.1). The design, calibration and operating procedure of the instrument are given elsewhere.[27] The load is measured by a strain gauge load cell, which has a sensitivity of 0.0002N, and penetration by a Linear Voltage Displacement Transducer (LVDT), the accuracy of which is measured to be ±0.08μm. The system is connected to a computer, in which a Labview based program controls and records data. Many micro-mechanical properties can be measured from a single dynamic indentation curve.

The indenter used for the analysis is a Brale diamond ball indenter with a tip diameter of 400μm (shown in Figure 2.2). It is ground, lapped and polished to control the conical angle to 120 ± 0.35 degrees. The spherical tip of the diamond cone should have a mean radius of 0.200 ± 0.010mm. The diamond indenter and the indenter holder are coaxial to within 0.5 degrees.

Each dynamic indentation is done to a maximum load of 1500g. A threshold value of 5g is used to eliminate the error arising from the noise in the machine. The indenter was driven at a rate of 0.2μm/sec. A 15 second dwell time was used at the maximum load. The compliance of the machine, determined by indenting a flat steel disk with a hardened steel punch, was estimated to be 0.006534μm/g and was subtracted from the indentation curves.

Since the sample surfaces were almost parallel, no mounting medium or sample holder is used while making measurements. Mounting media can result in some amount of bending by the specimen and can yield different results. The stage on which the sample is kept can be adjusted in all of the three directions x, y or z. Before every sample is indented, the height of the sample stage is adjusted (z-directional movement) so that the indenter tip just touches the sample surface. The initial 2 to 3 indentations were spent in bringing the instrument to "equilibrium" and were not taken for analysis. After making all the initial adjustments, each sample was indented 15 times for good statistical sampling of data.

Results obtained with the 400μm diameter indenter were compared with previous results obtained by Bowden, who used a 1mm diameter indenter. The total and final penetration depth values and more importantly plasticity values turned out to be significantly different. As a result, a decision was made to use a larger diameter indenter for quantitative comparison of results. A 2mm ball indenter, made of hardened steel, was chosen (shown in Figure 2.2).

Figure 2.1. The dynamic recording microindenter used for this study. Shown in the top of the picture is the PZT column with dual capacitance gauges. The spherical indenter, sample and the translatable stage are also shown.

Figure 2.2. Indenters used for dynamic micro hardness measurements. Shown in the left is the 2mm ball indenter with hardened steel tip. Shown in the right is the 400μm indenter with the diamond tip.

2.3 RESULTS AND DISCUSSION

2.3.1 LBH, DBH and Elastic Modulus

Different hardness values, elastic modulus and indentation energies are some of the properties calculated from the indentation curves. Loaded Brinell Hardness (LBH), which is calculated from the maximum load and maximum penetration depth, is given by the relation,

$$\text{LBH (GPa)} = \frac{P_{max}}{\pi D h_{max}} \tag{2.2}$$

where P_{max} is the maximum load in N and h_{max} is the maximum penetration depth in μm, which gives LBH the units of GPa.

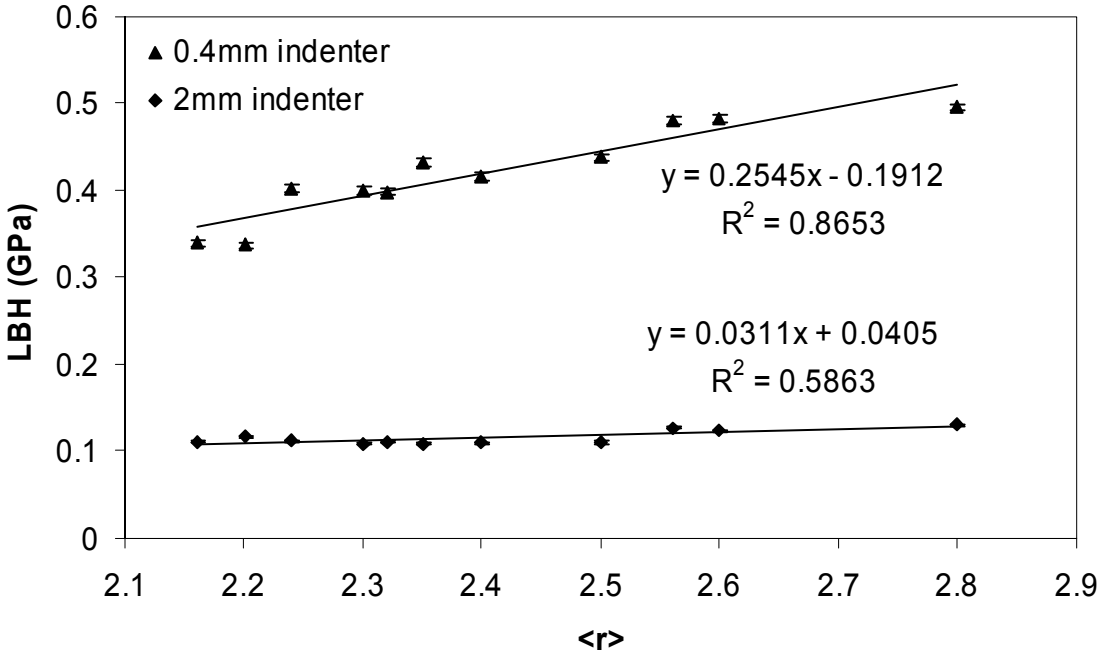

Figure 2.3. LBH vs <r> for the binary Ge-Se system shown for two indenters. A linear trend is observed in both cases. The values measured using 400μm indenter are considerably higher when compared to those using 2mm indenter.

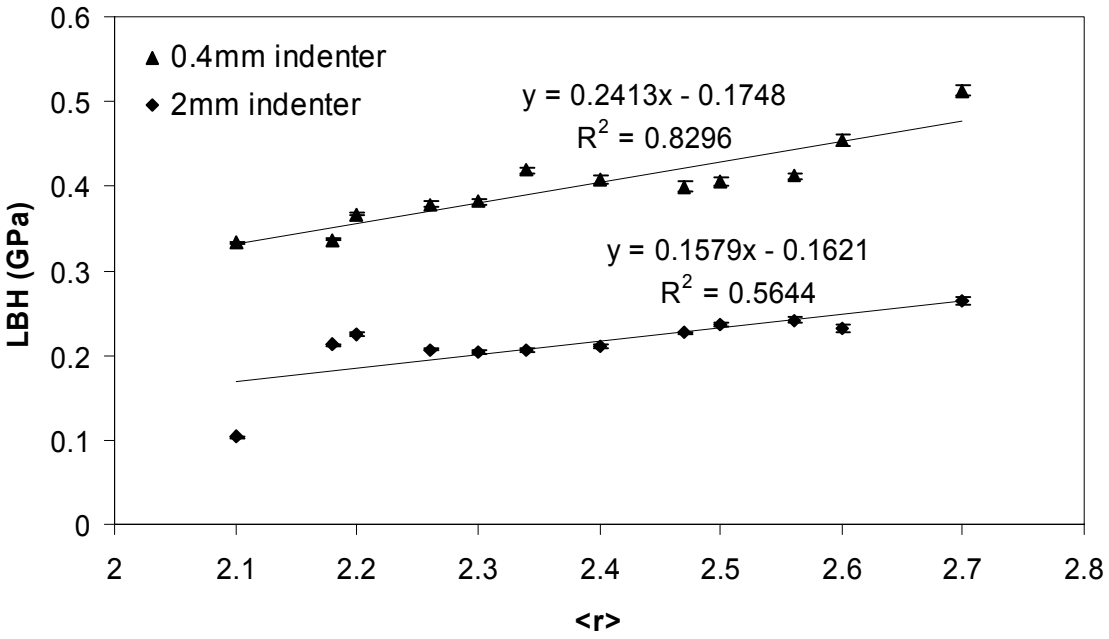

Figure 2.4. LBH vs <r> for the ternary Ge-Sb-Se system shown for two indenters. A linear trend is observed, with 400μm indenter giving higher values.

LBH, calculated from the above formula, is plotted as a function of the average coordination number <r> for binary and ternary glasses as shown in Figure 2.3 and Figure 2.4. Also shown is the comparison between the two indenters.

From the two graphs, it is clear that the value of LBH, increases with the average coordination number for binary as well as ternary glasses. As the coordination number increases, the maximum penetration depth created by the indenter decreases, which, in turn, increases the value of LBH. The trend observed here has already been discussed in detail elsewhere[15] and the primary goal is to compare the values obtained with different indenters.

One might expect the values of LBH obtained with a smaller indenter to be lower than that obtained with a larger indenter, since a smaller indenter creates higher penetration depth values. But this should not be true since the value of LBH also depends on the indenter diameter as shown in Equation 2.2. In this case, the values of LBH measured with the 400μm ball indenter are significantly higher than the values measured with the 2mm ball indenter, the reason for which is known. In order to

compare the results quantitatively, the LBH values obtained by Bowden with a 1mm ball indenter are also taken.[25] The relationships obtained with the three indenters for the Ge-Se binary system are given as follows.

$$\text{LBH (GPa)} = 0.2545\langle r\rangle - 0.1912 \quad (400\mu\text{m ball indenter})$$
$$\text{LBH (GPa)} = 0.085\langle r\rangle - 0.0206 \quad (1\text{mm ball indenter})$$
$$\text{LBH (GPa)} = 0.0311\langle r\rangle + 0.0405 \quad (2\text{mm ball indenter})$$

Clearly, $LBH_{400\mu m} > LBH_{1mm} > LBH_{2mm}$. Therefore, it is to be concluded that for both binary and ternary systems, *the values of LBH decrease as the indenter diameter increases*.

Dynamic Brinell Hardness (DBH), on the other hand, depends on the value of final penetration depth, as given by the relationship,

$$\text{DBH (GPa)} = \frac{P_{max}}{\pi D h_o} \tag{2.2}$$

where h_o is the final penetration depth in μm. The plot of DBH vs <r> is shown for both binary and ternary glasses in Figure 2.5 and Figure 2.6. The trend is almost similar to the one observed with LBH. DBH increases with the average coordination number for both binary and ternary systems, with 400μm ball indenter on the higher side. However, in the binary system, there is a local maximum observed in the curve at the physical threshold <r> = 2.4, for both indenters (400μm and 2mm), which is not the case with LBH. Since DBH depends on the value of final penetration depth (h_o), a higher value of h_o would lower the DBH value and vice versa. So, as stated by Firstenberg, a lower final/plastic penetration depth value or a higher preferential elastic recovery of glasses of the composition $Ge_{20}Se_{80}$, causes them to have a higher DBH value when compared to other glasses in the system.

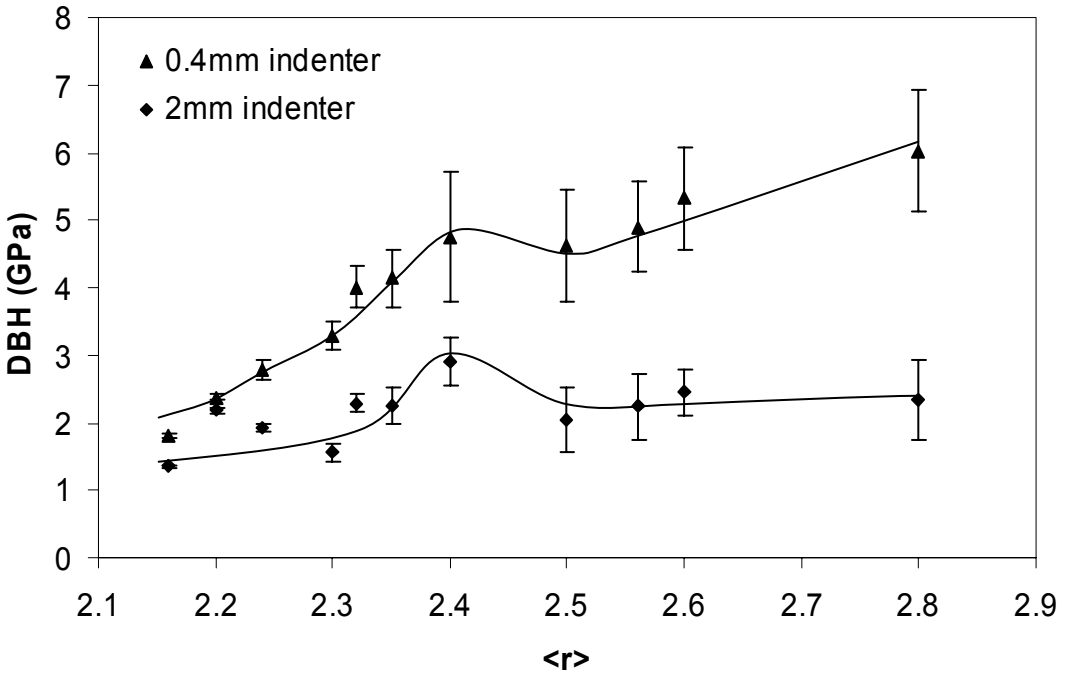

Figure 2.5. DBH as a function of <r> for the binary Ge-Se system, shown for both indenters. A hump is observed in the curve at <r> = 2.4.

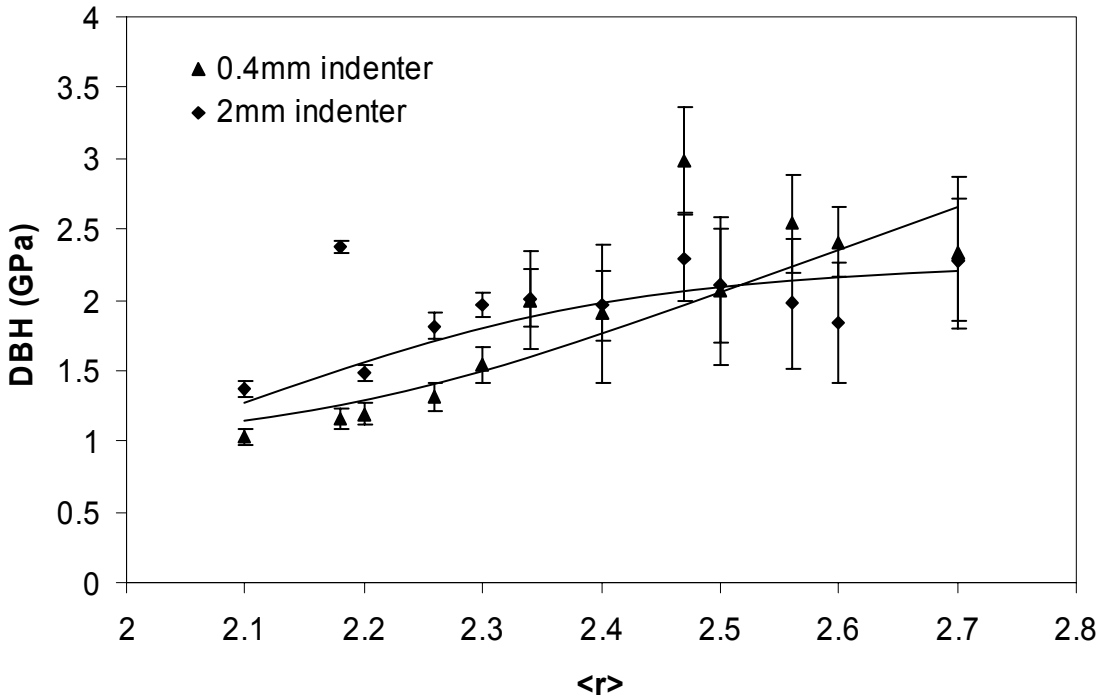

Figure 2.6. DBH as a function of <r> for the ternary system. No clear trend is observed except an increase in DBH value with <r>.

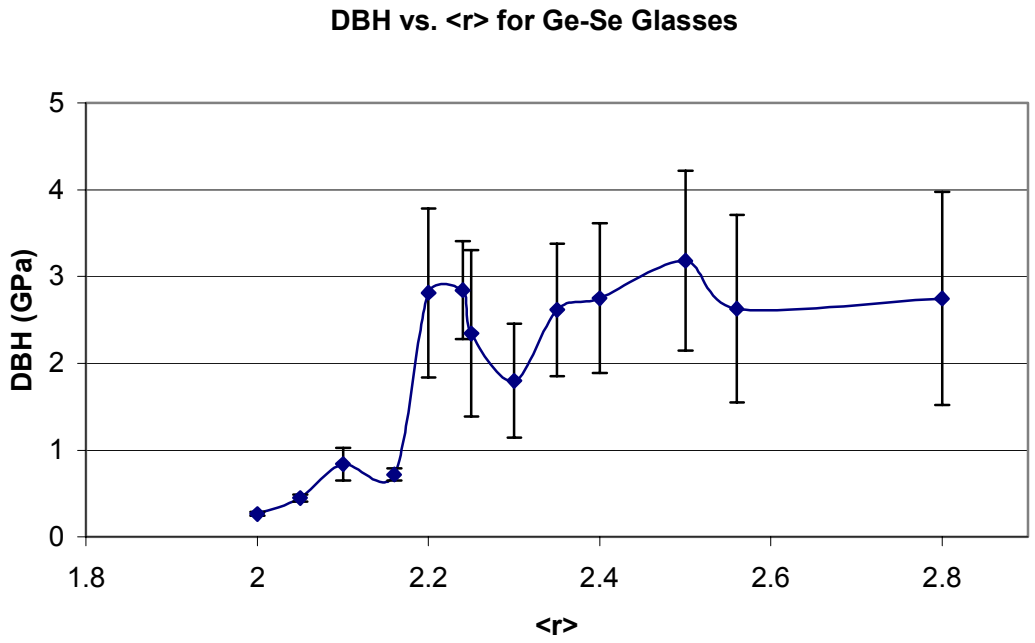

Figure 2.7. Values of DBH, plotted as a function of <r> for binaries, obtained with a 1mm indenter. Reproduced from Bowden.[25]

As already pointed out, the DBH values obtained in the binary Ge-Se system, with a 400μm ball indenter are higher than those obtained with a 2mm ball indenter. Lower coordination number glasses have DBH values close to each other, but the difference becomes considerable as the coordination number increases. On the other hand, no clear trend is observed for ternary glasses. In fact, for low coordination numbers, DBH values obtained with 400μm ball indenter seem to be lower than those obtained with 2mm ball indenter. This means that for low coordination number ternary glasses, the values of final penetration depth created by the 400μm indenter are quite high when compared to those created by the 2mm ball indenter. In other words, the plasticity created by the 400μm indenter for low coordination number ternary glasses should be considerably higher than that created by the 2mm ball indenter. The DBH values obtained with a 1mm ball indenter (from Bowden's thesis) for the Ge-Se binary system are also plotted in Figure 2.7 for comparison. The values seem to lie in between those obtained with 400μm and 2mm indenters.

Oliver and Pharr calculated the composite modulus, E_c, of the specimen-indenter system from the load-displacement curve through the equation,

$$E_c = \frac{S\sqrt{\pi}}{2\sqrt{A}} \tag{2.3}$$

where A is the area of plastic deformation and S is the slope of the initial part of the unloading curve.[28,29] In deriving the above equation, they assumed the contact area between the indenter and the specimen to remain constant during the initial withdrawal of the indenter. However, later analysis by King showed that the unloading stiffness is independent of the indenter geometry.[30]

The composite modulus, E_c, can also be given by,

$$\frac{1}{E_c} = \frac{(1 - \nu^2)}{E} + \frac{(1 - \nu_i^2)}{E_i} \tag{2.4}$$

where E and ν are the elastic modulus and Poisson's ratio for the specimen and E_i and ν_i are the same parameters for the indenter. From the above two equations, the equation for calculating the elastic modulus of the specimen can be written as,

$$E = \frac{(1 - \nu^2)}{\frac{2\sqrt{A}}{S\sqrt{\pi}} - \frac{(1 - \nu_i^2)}{E_i}} \tag{2.5}$$

Elastic moduli of the binary and ternary chalcogenide glasses are calculated using Equation 2.5. The plots are shown in Figure 2.8 and Figure 2.9. In both systems, E increases linearly with <r>, representing the increase in network connectivity and bond energy. In the binary system, the values obtained with 400μm ball and 2mm ball indenters are quite close. The 2mm ball indenter shows a very small local maximum around <r> = 2.4, but this can be considered inconclusive.

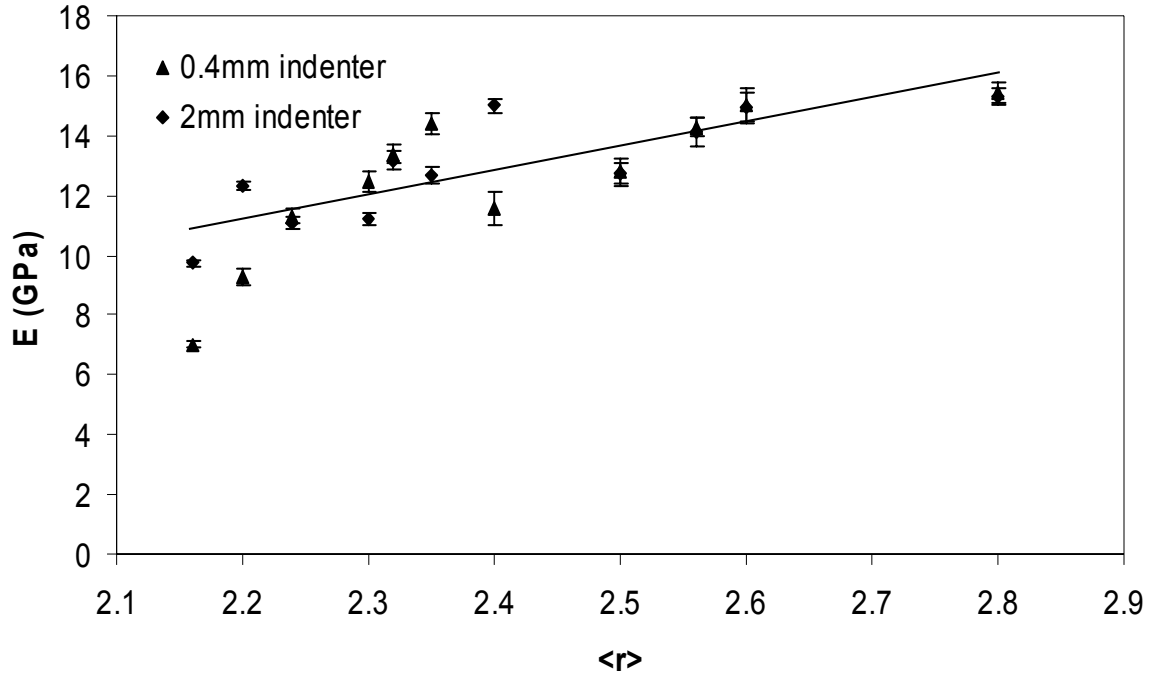

Figure 2.8. Elastic Modulus increases with network connectivity when plotted as a function of <r> for the binary Ge-Se system. Values obtained with both indenters are shown and the line is drawn as a guide to the eye.

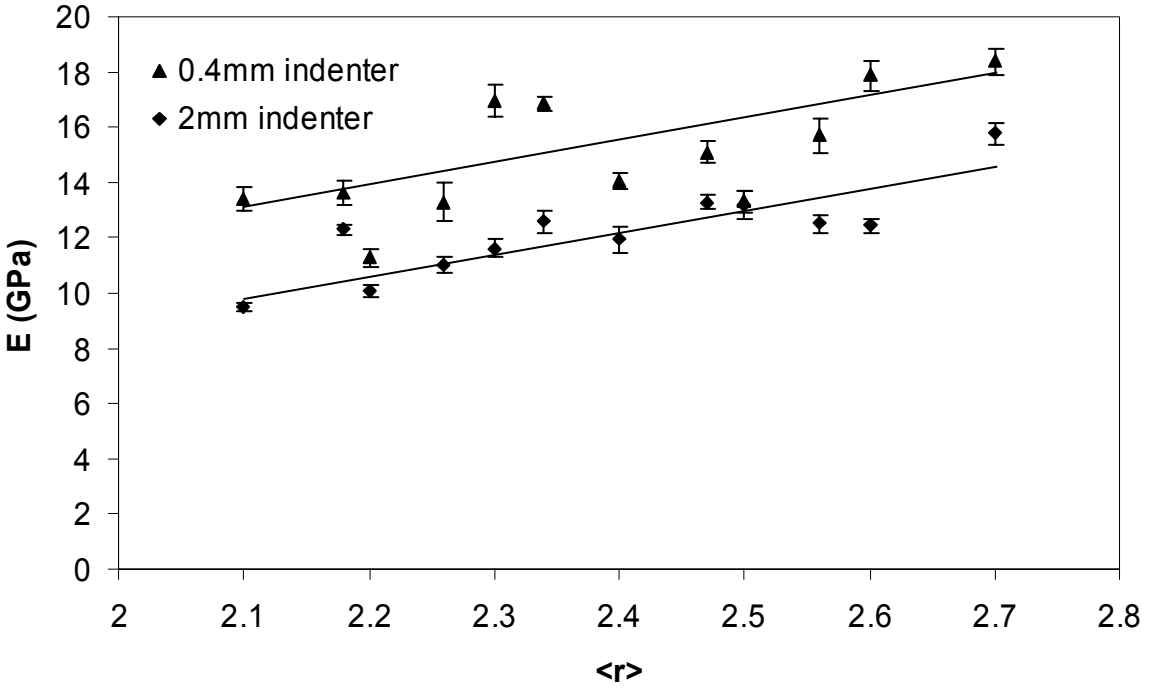

Figure 2.9. Elastic Modulus as a function of <r> for the ternary Ge-Sb-Se system. A similar trend is observed for both indenters.

A similar trend, i.e. a linear increase of elastic modulus with <r>, is observed in the ternary system. However, in order to study the difference in E values obtained with both indenters, linear equations are fit to the data. The 400μm ball indenter values are approximately 2GPa higher than those obtained by the 2mm ball indenter. Such high E values can be attributed to the higher initial unloading stiffness or lesser elastic recovery created by the 400μm ball indenter. Though the values of elastic modulus obtained by both indenters are slightly different, they fall in the same range of E values obtained by prior investigators.

Though there is some amount of scatter present in the elastic modulus values, when plotted as a function of <r>, it is expected to follow a linear trend due to the following reasons.

- Prior researchers have calculated the values of elastic modulus of glasses from <r> = 2.0 to <r> = 2.8 using ultrasonic velocimetry measurements and established a linear relationship between E and <r>. While ultrasonic velocimetry techniques do not involve any compression of the sample, dynamic indentations do. So, the deviation of E values from linearity could be attributed to the differences in the methods used.
- Several researchers have proposed different formulae for calculating the elastic modulus of specimens from dynamic indentation curves. The one proposed by Oliver and Pharr is based on the assumption that the indentation retains the geometry of the indenter during initial unloading. This could as well contribute to the deviations in data.
- Finally, the sensitivity of chalcogenide glasses to surrounding temperature changes, due to their very low glass transition temperatures, may play a major role as well.

2.3.2 Total and Elastic Energies of Indentation

In a typical load versus displacement curve, the area under the loading curve represents the total energy (E_t) measured during the indentation. The area under the unloading curve represents the energy that is recoverable elastically (E_e). The difference between the two curves is the unrecoverable plastic or hysteresis energy (E_h).

Measurement of the energies of indentation helps in understanding the effects of elasticity/plasticity created by the different indenters.

The total energy (E_t) is plotted as a function of <r> for both binary and ternary systems as shown in Figure 2.10 and Figure 2.11. In both systems, the total energy (E_t) decreases as the coordination number or the network stiffness increases. Also, in both systems, the total energy measured with the 400μm ball indenter is much higher than that measured by the 2mm ball indenter. Such high E_t values can be attributed to high penetration depths created by the 400μm ball indenter. For low coordination numbers, the difference is significantly high and it decreases as the coordination number increases.

The trends observed in the total energy values with respect to the average coordination number and indenter diameter can be studied simultaneously by plotting on a 3-D graph, such as the one shown in Figure 2.12. The data obtained using 1mm diameter indenter are taken from Bowden's thesis.[25] Changes in E_t values with respect to <r> are joined separately for different indenters. Another important observation is that the total energy decreases as the indenter diameter increases. An arrow pointing downwards indicates this.

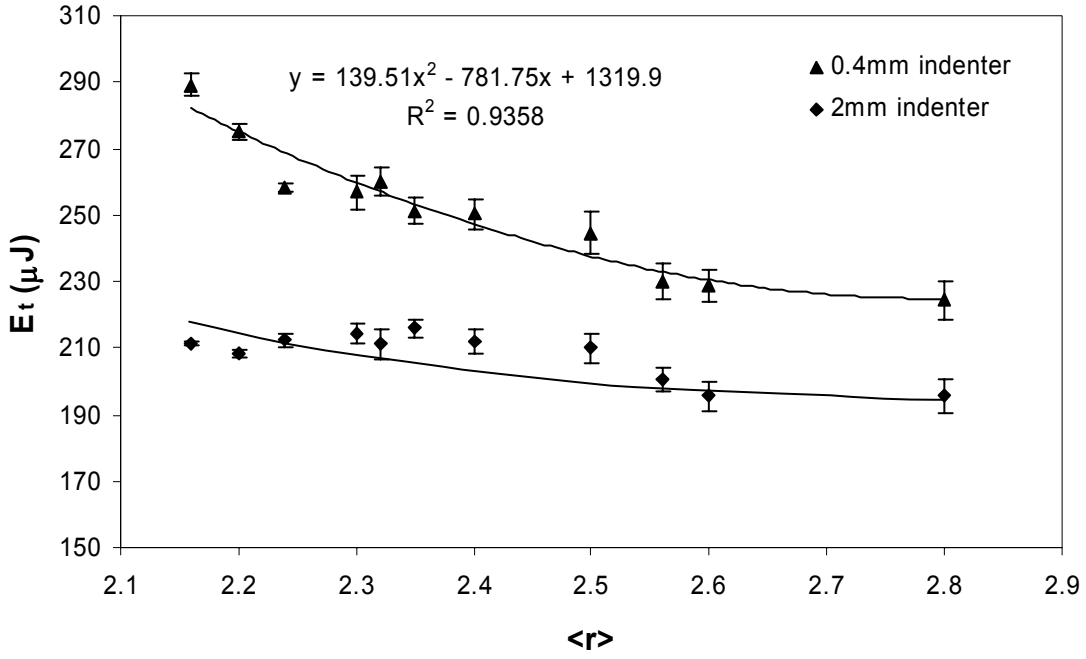

Figure 2.10. Total energy as a function of the coordination number for the binary Ge-Se system. E_t decreases as the connectivity of the network increases. Also shown is the comparison between two indenters.

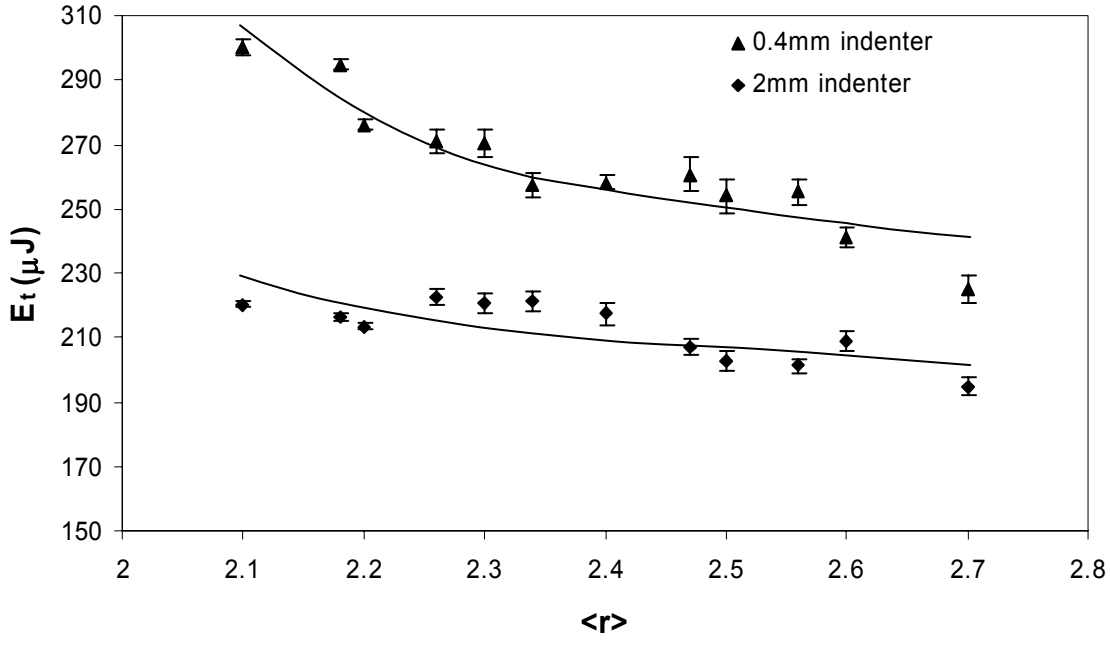

Figure 2.11. E_t Vs <r> for the ternary Ge-Sb-Se system for both indenters. A similar trend is observed.

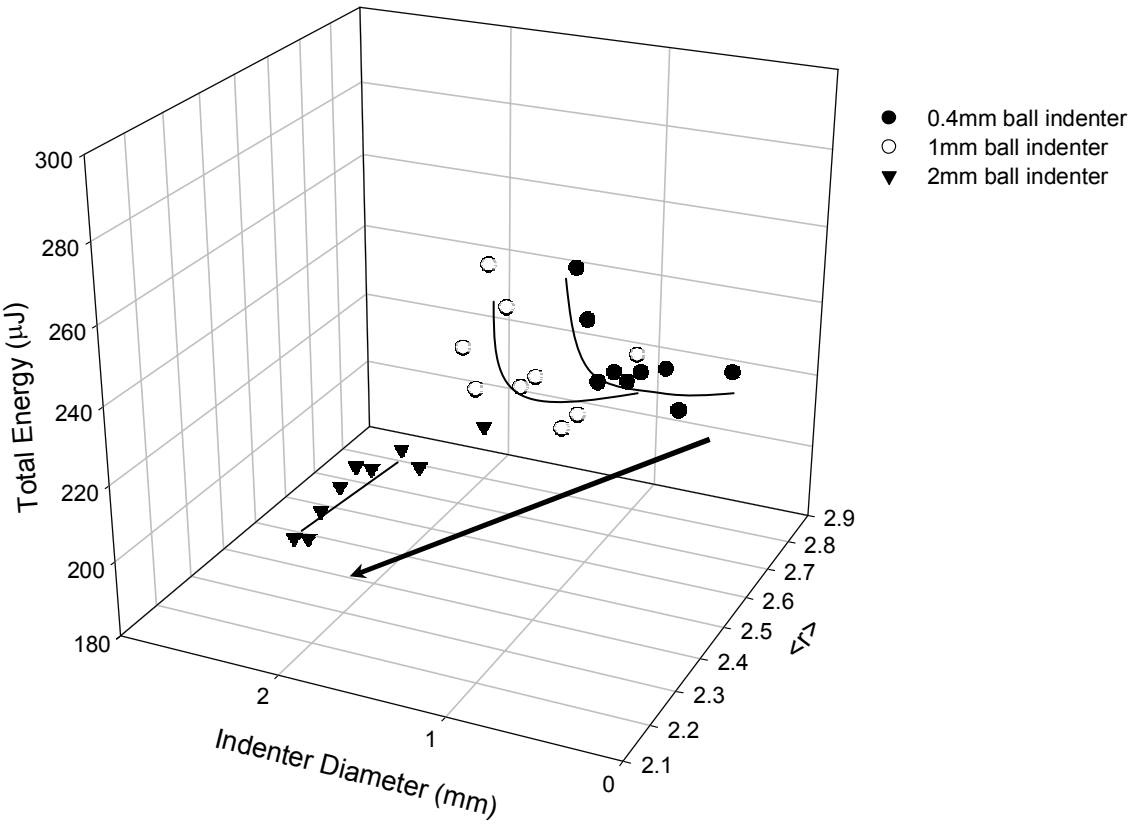

Figure 2.12. Changes in total energy with respect to both the indenter diameter and coordination number for the binary system. The data obtained by three indenters are separately joined. The arrow points towards the direction of decreasing total energy with increasing indenter diameter.

Elastic energy is normalized to total energy and plotted as a function of <r> for both binary and ternary systems as shown in Figure 2.13 and Figure 2.14. In both systems, the value of normalized elastic energy increases as the coordination number increases. However, in the binary system, the elastic energy approaches a shallow maximum at the physical threshold, <r> = 2.4. It is already seen that the value of DBH approaches a maximum at <r> = 2.4. In the ternary system, there may be a shallow maximum closer to <r> = 2.6.

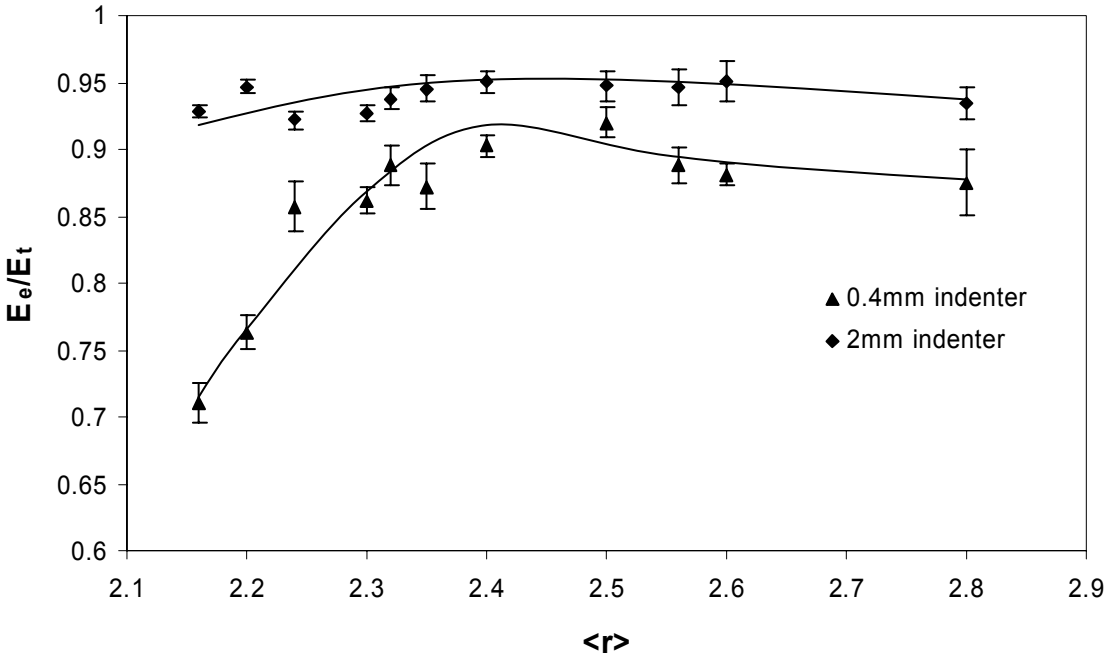

Figure 2.13. Normalized elastic energy is plotted as a function of the average coordination number for the binary Ge-Se system. A broad hump is noted at <r> = 2.4 for both indenters.

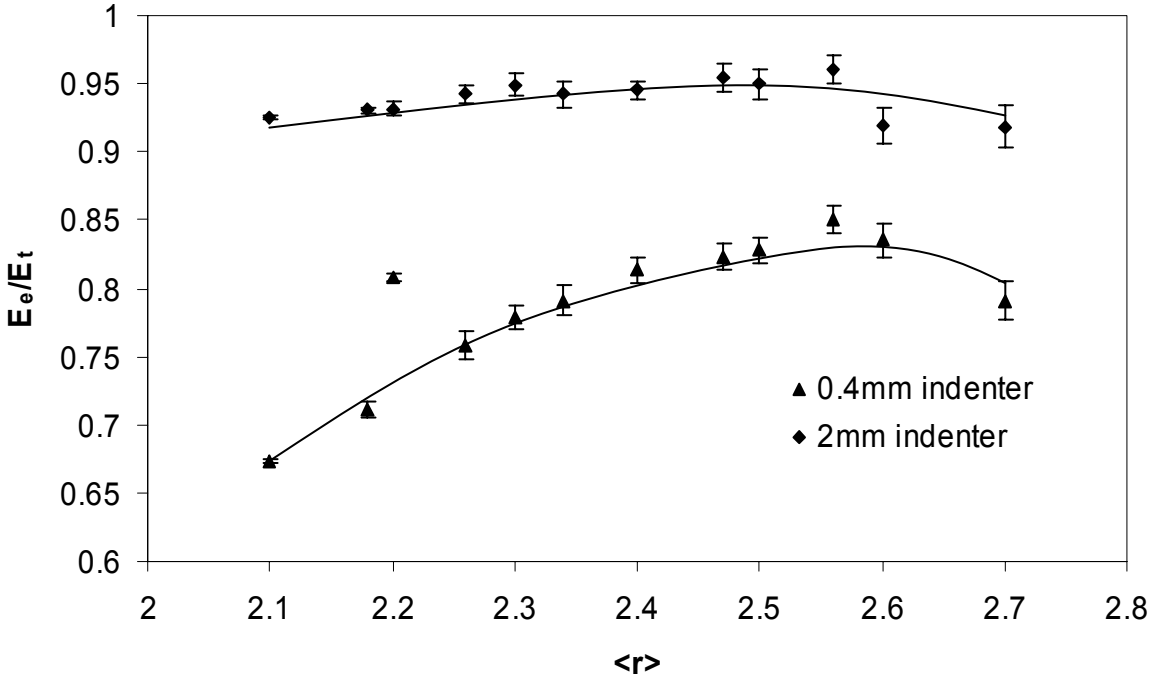

Figure 2.14. Normalized elastic energy is plotted as a function of <r> for the ternary system. No such trend is observed.

Another important observation is that the values of normalized elastic energy obtained with the 2mm ball indenter are higher when compared to the 400μm indenter. This makes sense since a larger diameter indenter does create lesser total and final penetration depths than a smaller diameter indenter. By plotting a 3-D diagram such as the one shown in Figure 2.15, the effects can be best understood. The values of normalized elastic energy increase as the coordination number increases and approach a maximum at <r> =2.4 in the binary system. A similar trend is observed for all the three indenters. Also, the values of E_e/E_t increase as the indenter diameter increases. An arrow pointing upwards indicates this. Values for 1mm indenter are taken from Bowden's thesis.[25]

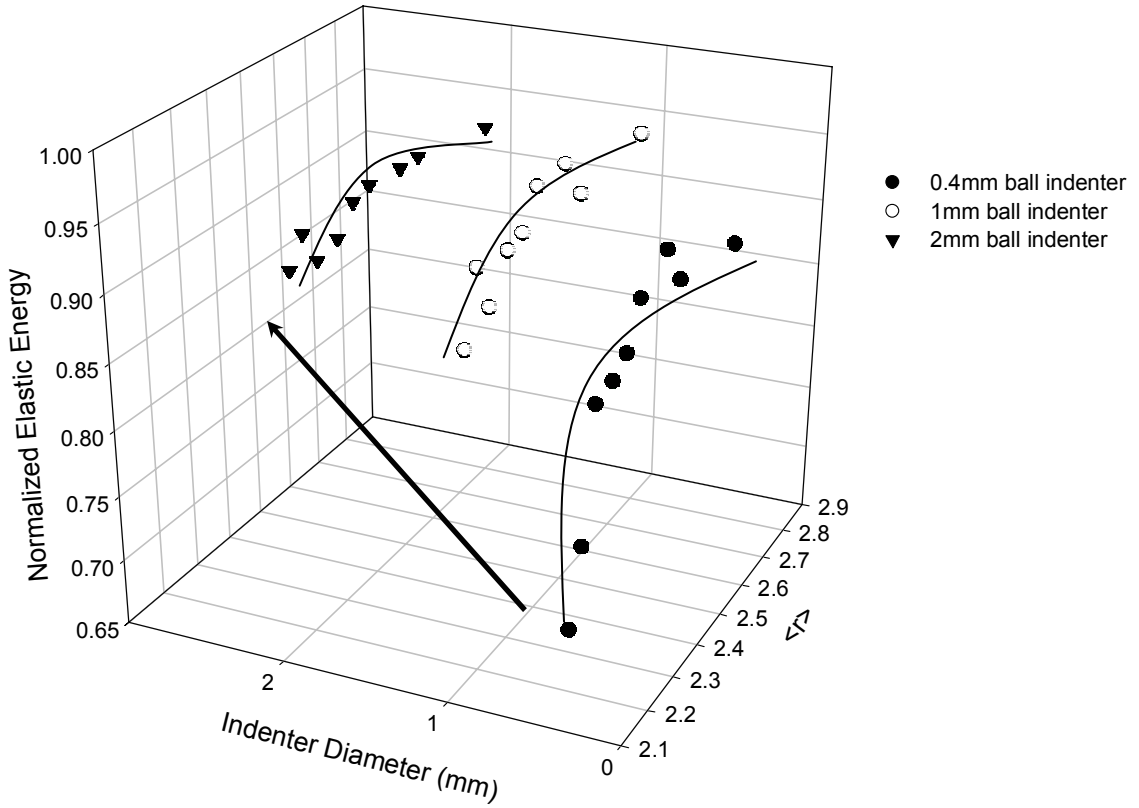

Figure 2.15. Normalized elastic energy is plotted with respect to both the indenter diameter and <r> for the binary system. Values obtained with different indenters are separately joined. Arrow is pointing towards the direction of increasing elastic energy with indenter diameter.

2.3.3 Trends Observed in Normalized Plasticity Values

As already mentioned, the difference between the total energy and elastic energy represents plastic energy. Values of plastic energy are normalized to total energy and plotted as a function of coordination number for both systems as shown in Figure 2.16 and Figure 2.17. For both systems, the values of normalized plastic energy decreases as the coordination number increases. Also important are the values obtained with different indenters. The difference between the values obtained with both indenters is high for low coordination numbers and decreases as <r> increases. It is clearly seen that a 400μm ball indenter creates higher plasticity when compared to a 2mm ball indenter. In fact, the values obtained for low coordination numbers using 400μm ball indenter are approximately two times higher than those obtained with the 2mm ball indenter. Normalized plastic energy versus <r> versus indenter diameter is shown in Figure 2.18. Unsurprisingly, the values of normalized plastic energy decrease as the indenter diameter and coordination number increase. Values for 1mm indenter are taken from Bowden.[25]

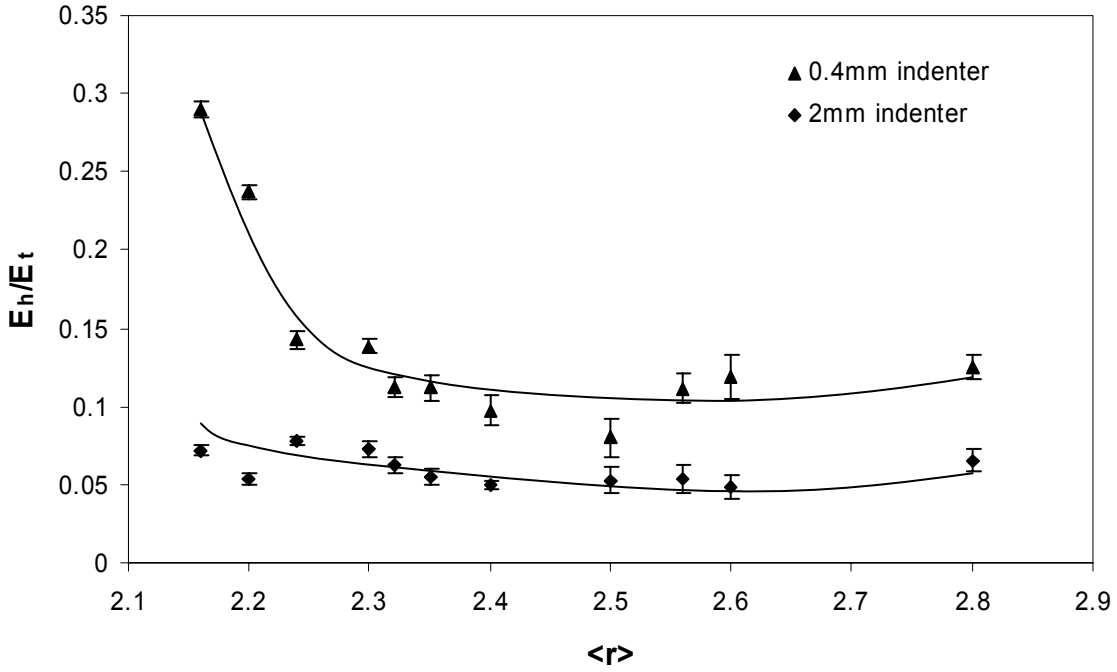

Figure 2.16. Normalized plastic energy decreases down the line, when plotted as a function of <r>, for the binary system.

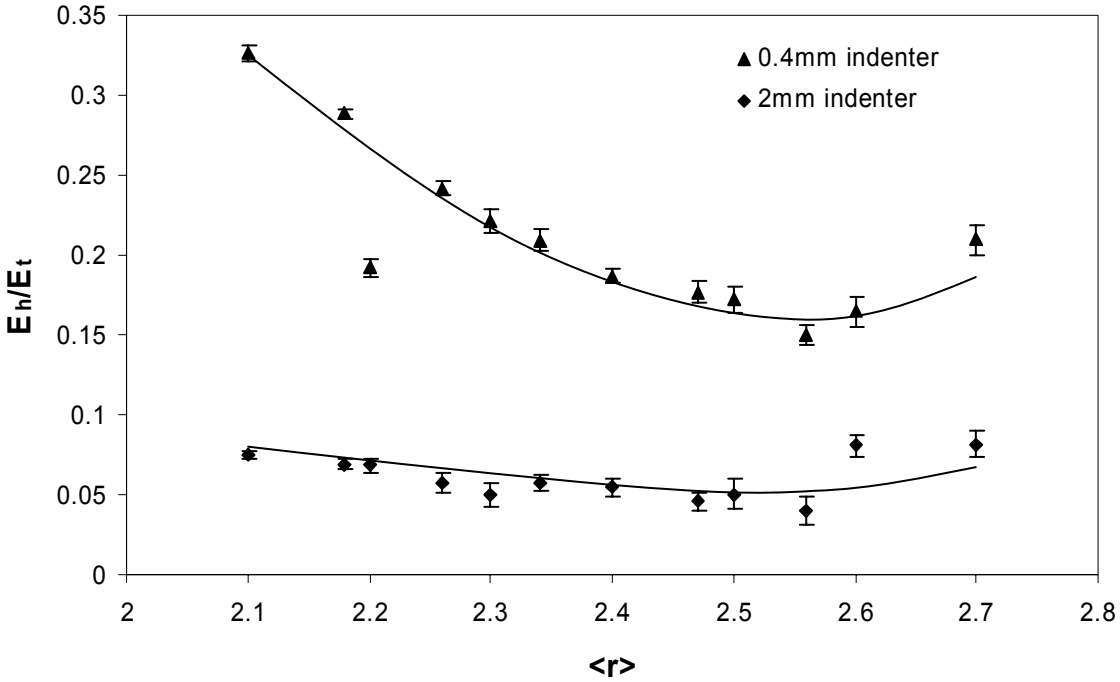

Figure 2.17. Normalized plastic energy is plotted as a function of <r> for the ternary system. A similar trend is observed for both indenters.

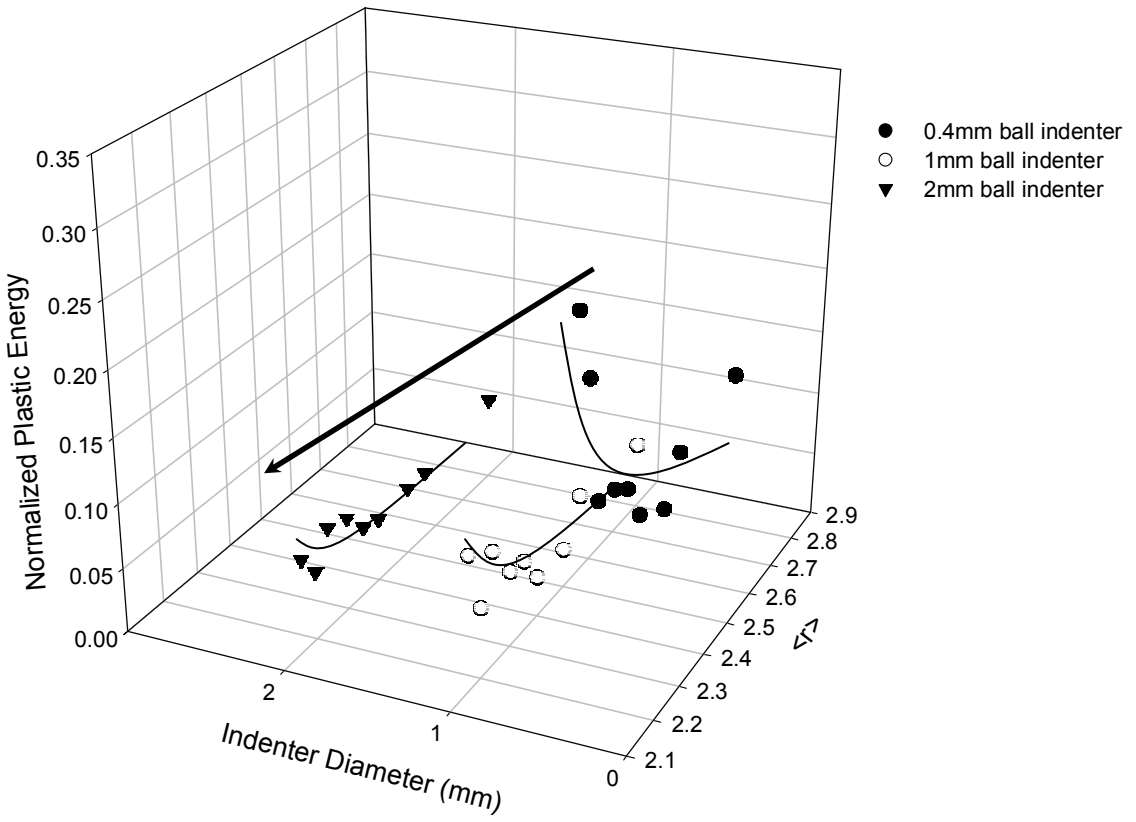

Figure 2.18. Normalized plastic energy is plotted with respect to both the indenter diameter and <r> for the binary system. Arrow points towards the direction of decreasing plastic energy with increasing indenter diameter.

The trends observed with elastic and plastic energies normalized to total energy explain the behavior of different indenters. Another valid comparison would be to compare the plasticity to elasticity ratio created by different indenters, which, in turn, estimates the percentage of plasticity or elasticity for a specific coordination number created by different indenters. Such a plot is shown in Figure 2.19 for the binary Ge-Se system. The trend is similar to the one observed with normalized plastic energy. The plasticity/elasticity ratio decreases as the indenter diameter and coordination number increase. A very important observation is that glasses of the coordination number 2.4 have the *lowest plasticity/elasticity ratio* when compared to other glasses. This is observed with all the indenters. This means that glasses of the coordination number 2.4 not only show a high elastic recovery, but also have the lowest percentage of plasticity in the system. Again this can be explained by the fact that they have the lowest h_o/h_{max} (the ratio of final to total penetration depth) value in the system.

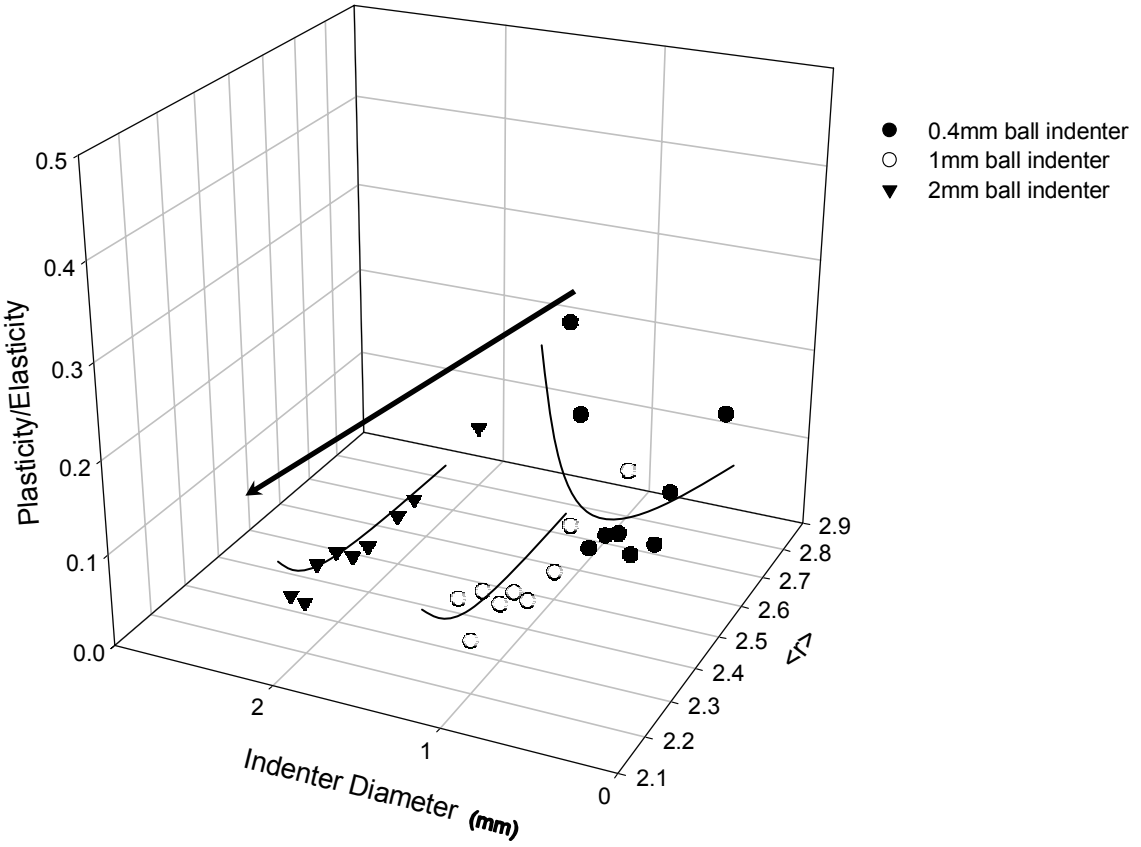

Figure 2.19. The ratio of plasticity to elasticity is plotted as a function of both the indenter diameter and the coordination number for the Ge-Se binary system. Arrow points towards the direction of decreasing plasticity/elasticity ratio with increasing indenter diameter. Values for 1mm indenter are taken from Bowden.

2.3.4 Energy Recovered or Consumed Normalized to Total System Energy of the Network

All the energy calculations performed above are based on the assumption that all the atoms in the network contribute to the resistance against the indentation. This is not exactly the case since the indentation is done only in a small region of the sample. Bonds would be broken and the structure would be densified only in those regions where the indenter contacts the sample. So, the calculation of the contact area of the indenter, and the penetration volume of the indenter would help in estimating the number of atoms being displaced by the indenter. Therefore, the energy calculations were performed taking in to account the total system energy of the network.

For a spherical indenter, the contact area can be given by the following equation,

$$A = \pi(Dh - h^2) \tag{2.6}$$

where D is indenter diameter and h is its penetration depth.[31] Integrating the above equation between the limits 0 and h, the volume being penetrated by the indenter is given by,

$$V = \pi\left(\frac{Dh^2}{2} - \frac{h^3}{3}\right) \tag{2.7}$$

Equation 2.7 is used to calculate the indentation volume. The plastic energy normalized to the total system energy is plotted for both binary and ternary systems as shown in Figure 2.20 and Figure 2.21. The density data required for the calculations are taken from a paper by Senapati et al.[32] Total system energy is calculated as the sum of total energy of indentation (E_t) and the total covalent bond energy of the network. The densification component of plastic deformation increases with <r> and so is the covalent bond energy of the network. As expected, the plastic energy normalized to the total system energy decreases as the coordination number increases. The plastic component of the total indentation energy decreases rapidly (elastic energy increases rapidly) till <r> = 2.4 and a slight increase is observed at higher coordination numbers. The same effect is observed with both indenters with 400μm ball indenter giving higher values. Since the indentation volume is proportional to the diameter, a larger diameter indenter would create a higher penetration volume than a smaller diameter indenter. So, the number of atoms displaced by the 2mm ball indenter would be higher than that displaced by the 400μm ball indenter.

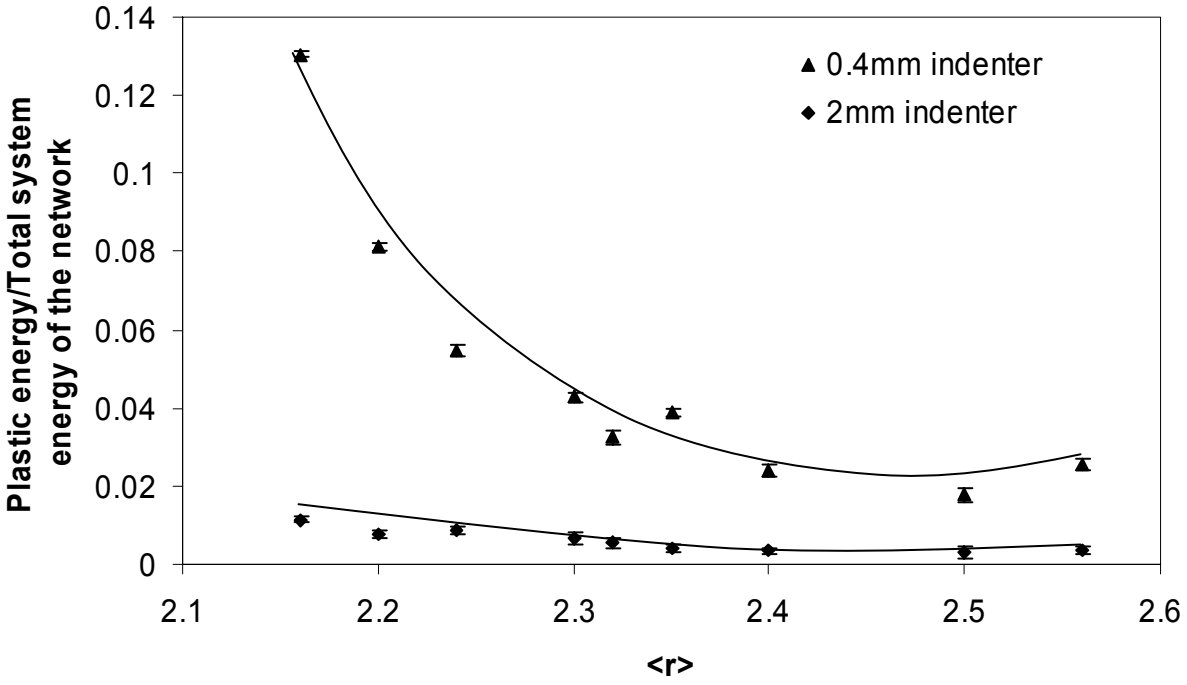

Figure 2.20. Plastic energy normalized to total system energy of the network for different indenters as a function of <r> for the binary system.

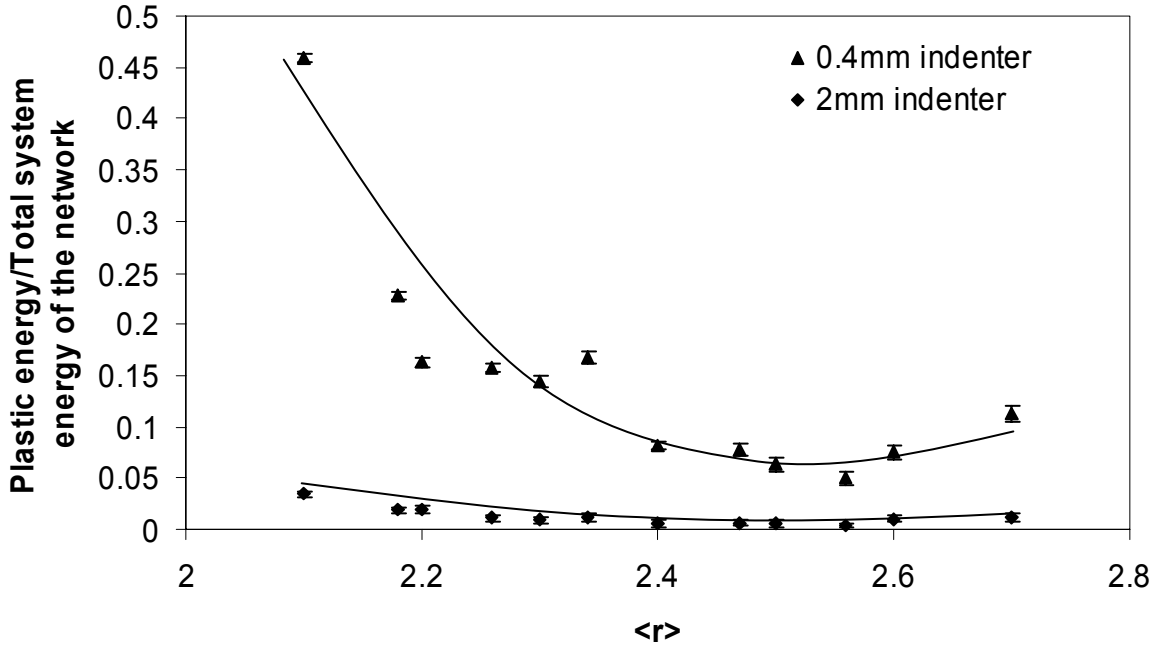

Figure 2.21. Plastic energy normalized to total system energy of the network for different indenters as a function of <r> for the ternary system.

To summarize, the total and plastic energies decrease as the indenter diameter and the coordination number increase. Elastic energy increases as <r> increases showing a local maximum <r> = 2.4. The calculation of energies consumed/recovered normalized to total system energy of the network shows similar trends for both binary and ternary systems. The consumed plastic energy normalized to total system energy of the network decreases rapidly till <r> = 2.4. However, there is a slight increase observed in the values at higher coordination numbers. This is more pronounced in the ternary system. The plastic component of indentation energy observed with a 2mm ball indenter is lower than that observed with the 400μm ball indenter.

3 STATIC INDENTATION MEASUREMENTS

3.1 ROOM TEMPERATURE MEASUREMENTS

3.1.1 Experimental Procedure

Since the dynamic micro-indentation measurements showed extrema at <r> = 2.4 in properties such as DBH and E_e, static indentations were performed to find extrema, if any, in properties such as indentation toughness or brittleness as observed by Strange.[16] A Buehler Micromet II hardness tester fitted with a Vickers' diamond tip was used for making the measurements. Each sample was indented with loads of 50, 100, 200, 300, and 500g. The loading time was 15 seconds in order to include the observations of possible viscous flow and plastic deformation. The resulting impressions and crack diagonals were measured using a video microscope. A Hitachi KP-D50 digital video camera connected to a digital image capture system was used for observing the indentations. Measurements were done using Image Pro Plus 3.0 image analysis software. Before the actual measurements were carried out, the system was calibrated using a micrometer slide.

After each indentation, the crack lengths (C_1 and C_2) and indentation diagonals (a_1 and a_2) were measured. Both of them are averaged for calculations. There exists some difficulty in measuring the exact length of cracks if they are at a slight angle to the indentation diagonal. In those cases, measurements were done parallel to the indentation diagonal. The longest crack is always chosen for the measurement. Most importantly, if no cracks are seen around indentation corners, then the crack length is assumed to be of the same length as the indentation diagonal.

3.1.2 Results and Discussion

Vickers Hardness Number, calculated from the applied load, P and the indentation diagonal, a is given by the equation,

$$VHN\ (GPa) = 1.854\ P/a^2 \qquad (3.1)$$

VHN is plotted as a function of <r> in Figure 3.1, just to confirm the expected linear trend. It is approximated by the relationship,

$$VHN\ (GPa) = 1.9541\langle r\rangle - 3.4589 \qquad (3.2)$$

which is quite close to the relationship shown in Figure 1.3.

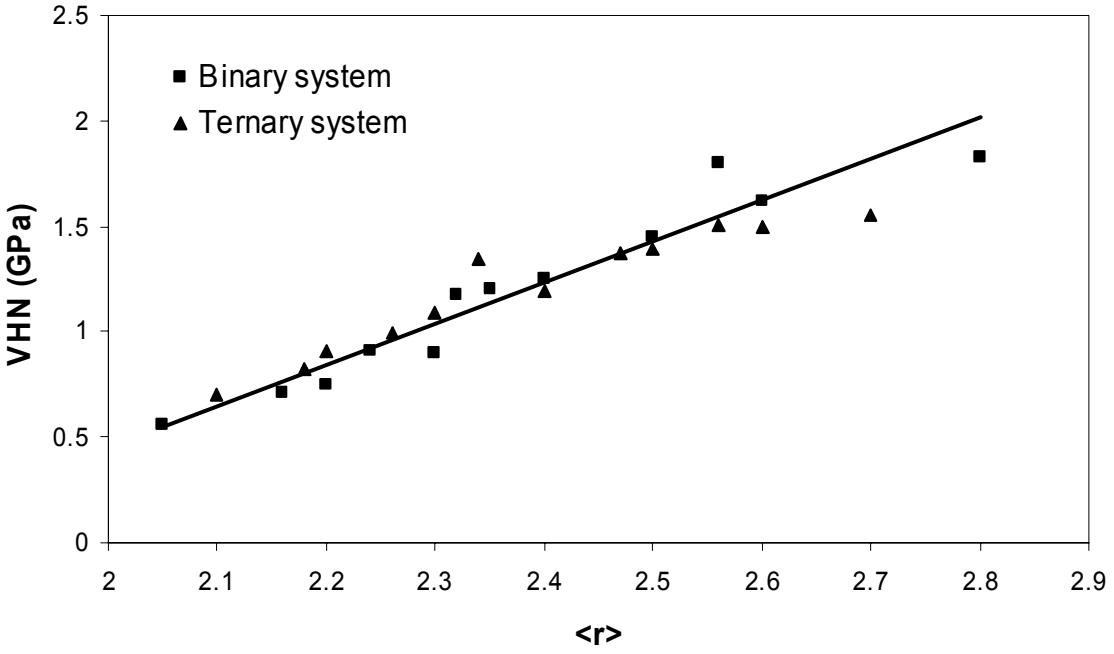

Figure 3.1. VHN vs <r> plot for Ge-Se and Ge-Sb-Se systems.

Fracture toughness, K_c, and brittleness, B, can be calculated using the indentation diagonal and crack length measurements. Fracture toughness is calculated using the equation proposed by Anstis et al.,[33]

$$K_c = \S_V^R \quad (E / H)^{1/2} (P / c_o^{3/2}) \qquad (3.3)$$

where § is a material independent constant for Vickers produced radial cracks (= 0.016), c_o is the average length of the radial crack in metres, E and H are the Young's modulus and hardness of the material in MPa, which gives K_c the units of MPa$\sqrt{m}$.

Lawn and Marshall,[34] in 1979, defined brittleness as the ratio of hardness to fracture toughness (H/K), from which Sehgal et al. developed the expression,[35]

$$B = (1/0.0056)^{3/2} (c_o/a)^{3/2} P^{-1/4} \quad (3.4)$$

Brittleness and fracture toughness, calculated using the above equations were correlated to compositions to observe any property threshold. The brittleness was found to attain a minimum at $Ge_{20}Se_{80}$ and the fracture toughness maximized at the same composition. Low coordination number glasses have glass transition temperatures close to room temperature. So, in order to have only structural factors, and not thermal factors, contributing to trends in data, indentations were then performed at –80°C.

3.2 INDENTATIONS AT –80°C

3.2.1 Experimental Procedure

Cold indentations were performed at –80°C using methanol and liquid nitrogen. An aluminum receptacle was fabricated for this purpose. The inner bath was filled with methanol (Mallinckrodt AR grade), which was chilled to its freezing point (–97.6°C) by slowly adding liquid nitrogen in the outer bath. A plastic extension rod was used to extend the Vickers diamond tip. A type T thermocouple was used to record the temperature. Indentations were performed at –80°C and continued as the temperature increased, one indentation every 3 degrees centigrade, till it reached the room temperature.

3.2.2 Results and Discussion

The plots of brittleness versus <r> for the binary and ternary systems are shown in Figure 3.2 and Figure 3.3. Binary glasses of the composition $Ge_{20}Se_{80}$ have the lowest brittleness in the system for both room temperature data and cold indentation data. This suggests that the structural consideration of optimized connectivity, which is making them resistant to fracture, is independent of temperature. The brittleness is high for low coordination number glasses until it drops down to a minimum at <r> = 2.4. It increases again drastically to a maximum at <r> = 2.8. The cold indentation data for low coordination number glasses differ much from room temperature data when compared to high coordination number glasses. This means that the "chilling" significantly increased the hardness and brittleness of the low coordination number glasses while high coordination number glasses are less affected by it. However, as seen in Figure 3.3, no clear trend is observed for ternary glasses.

Plot of indentation toughness, calculated at room temperature, versus <r> is shown in Figure 3.4 for the binary and ternary systems. Again, a maximum is observed in K_c at <r> = 2.4 for the binary system. Glasses below and above <r> = 2.4 have values far below 0.8 MPa $m^{1/2}$ such that the K_c value of $Ge_{20}Se_{80}$ is almost twice or thrice that of other glasses. However, calculated values for ternary glasses are very low and no clear trend is observed. Indentation toughness calculations performed for the cold indentation data also show similar results.

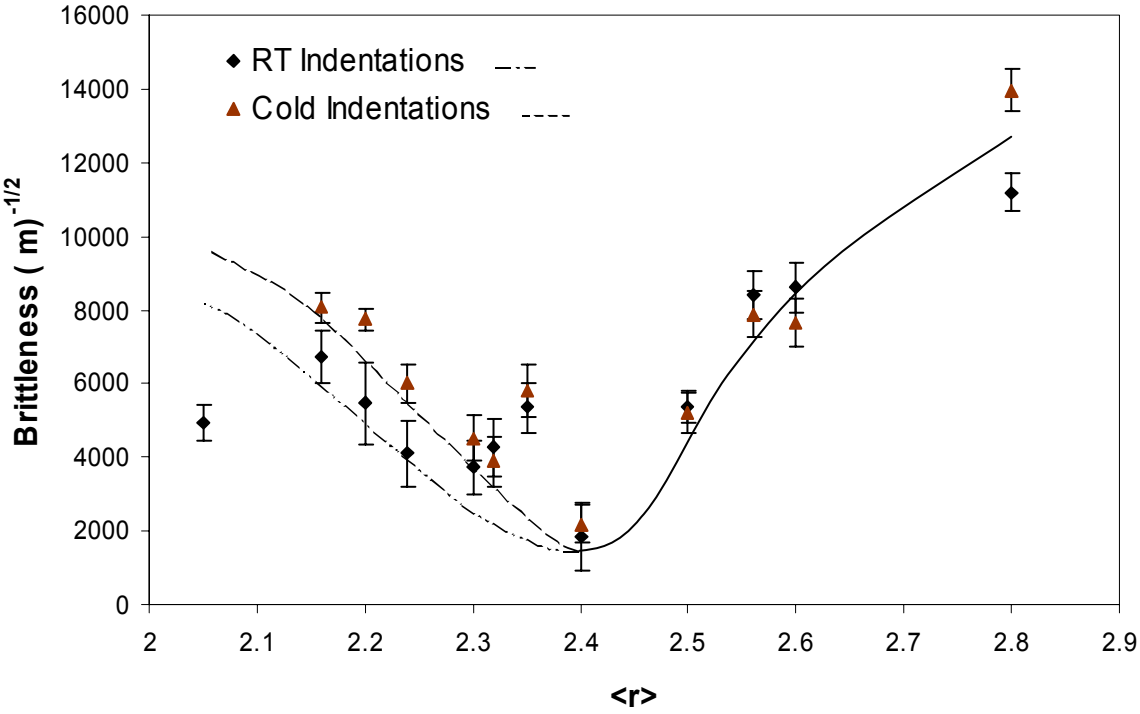

Figure 3.2. Brittleness is plotted as a function of <r> for the Ge-Se binary system. A minimization is observed at <r> = 2.4 at room temperature as well as at –80°C. RT stands for Room Temperature. Brittleness values for RT indentations and cold indentations are slightly different for low coordination number glasses, which are joined by separate curves.

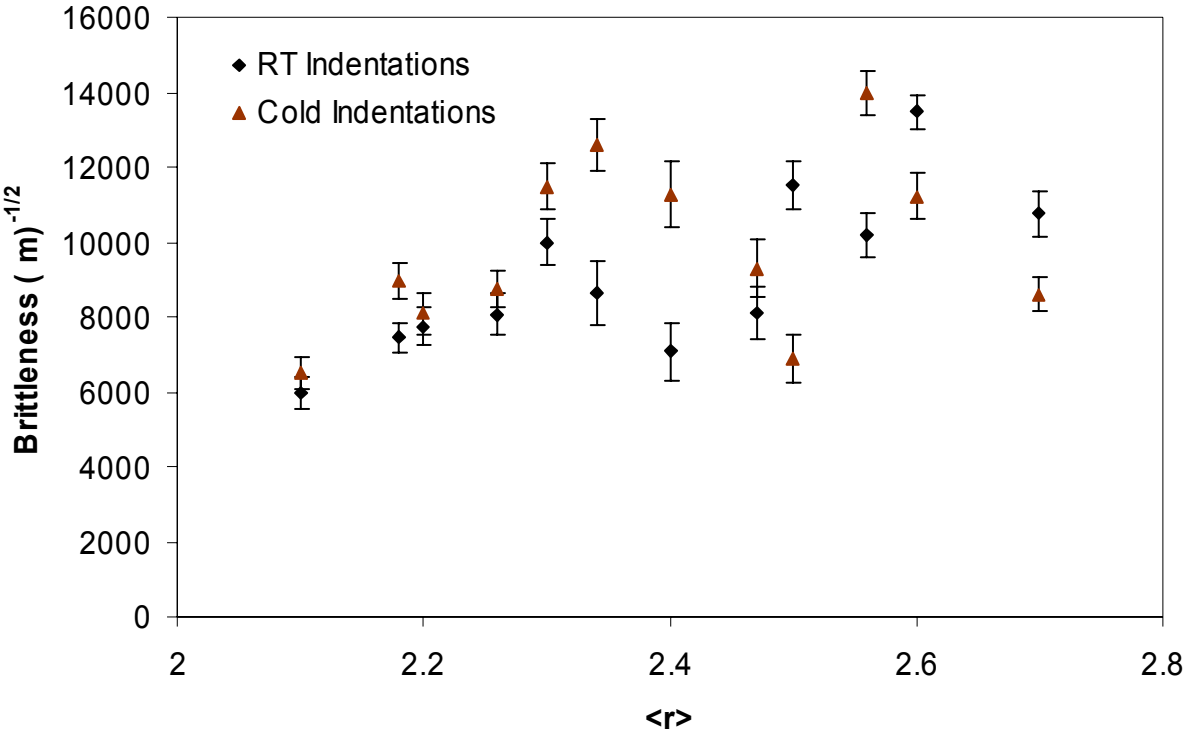

Figure 3.3. Brittleness is plotted as a function of <r> for the Ge-Sb-Se system. No clear trend is observed.

Since the K_c value for the $Ge_{20}Se_{80}$ glass was very much higher than those of other glasses, two other samples of the same composition (US* and DS** as shown in Figure 3.4) were chosen to verify the results. The sample labeled DS is ~4 years old and the other sample labeled US is ~ 8 years old. Both of them also showed very high toughness values. This leads to the conclusion that binary glasses of the coordination number 2.4 show very high toughness values with little changes over time.

So far, it is seen that binary glasses of the coordination number 2.4 have maximum K_c, E_e and DBH. Strange[16] attributed this to the observed minimum in brittleness. Firstenberg[15] attributed the same to the high plastic yield strength of those glasses. In order to understand the mechanics, which leads to extrema in properties, a finite elemental simulation was performed.

* Glass melted by U. Senapati
** Glass melted by D. Strange

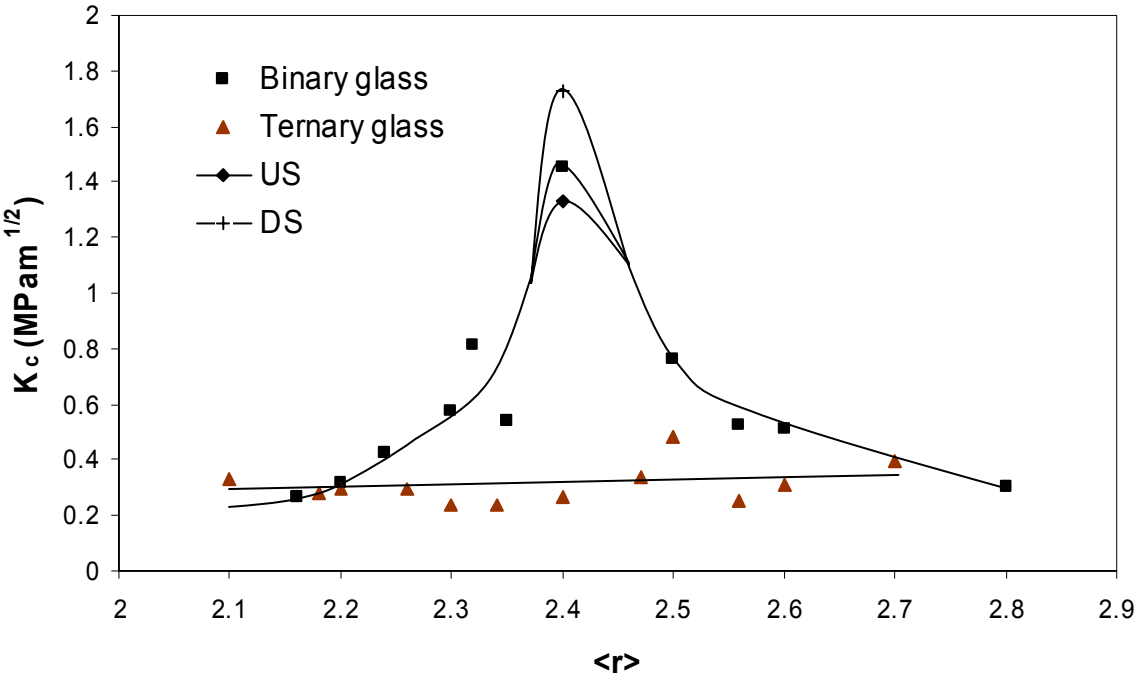

Figure 3.4. Fracture toughness, measured at room temperature, is plotted as a function of <r> for both binary and ternary systems. Maximization occurs at <r> = 2.4 for the binary system. No such trend is observed in the ternary system. DS and US represent the <r> = 2.4 binary glass samples made by two prior investigators.

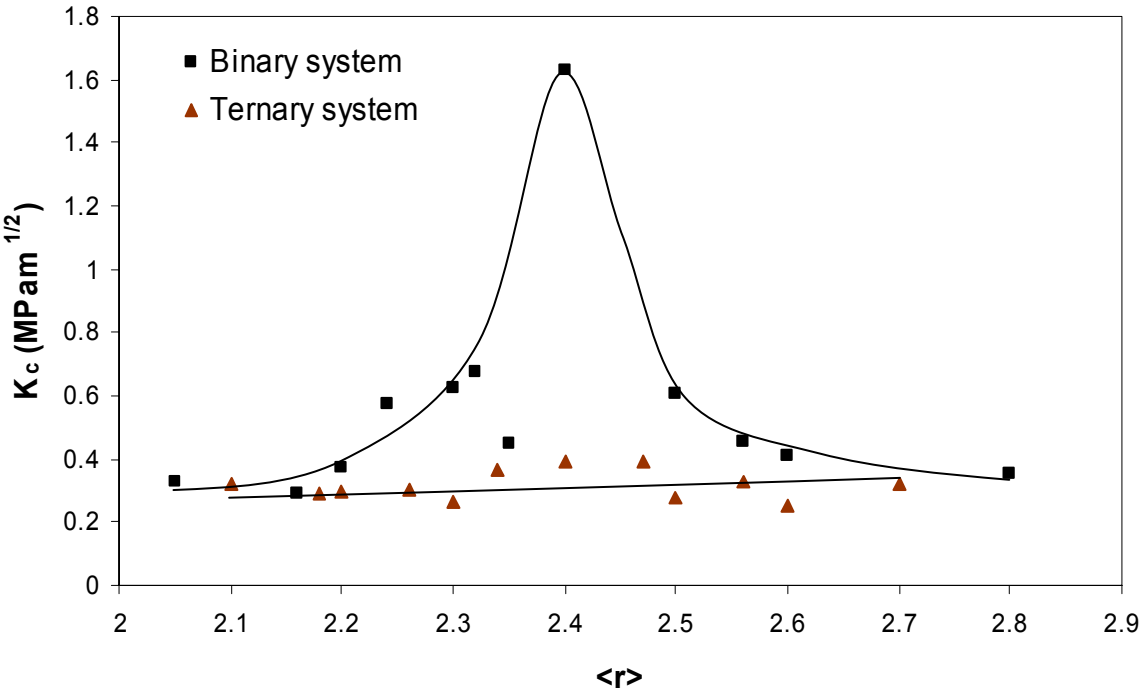

Figure 3.5. Fracture toughness, measured at –80°C, is plotted as a function of <r> for both binary and ternary systems. A similar maximization is observed at <r> = 2.4 for the binary system.

4 FINITE ELEMENT ANALYSIS OF INDENTATION

4.1 INTRODUCTION TO CONTACT MECHANICS

A fundamental problem in the mechanics of materials is the contact between two non-conforming bodies. Examples include the friction and wear of engineering solids, powder compaction processes which rely upon the plastic indentation of deformable particles for their success, indentation tests to measure the elastic/plastic properties of materials and so on. Spherical indentations, using a steel ball, have been in play since Brinell introduced it in 1901. Recently, load-depth sensing micro-indenters using diamond spherocones, from which representative stress-strain curves can be produced, have been developed. They can also be coupled with finite element method to investigate strain hardening behavior of materials.

Hertz was the first to analyze the stresses at the contact of two elastic solids. He derived the basic relationship between displacement (h), and force applied to an indenter (P), namely,[36]

$$h = (3P/4E_r)^{2/3}(1/R)^{1/3} \tag{4.1}$$

where R is the nominal radius of the indenter tip and E_r is the reduced modulus which is related to the elastic modulus of the sample, E, through the elastic modulus of the indenter, E_i, and Poisson's ratio of the indenter, ν_i, and the sample ν by,

$$\frac{1}{E_r} = \frac{(1 - \nu^2)}{E} + \frac{(1 - \nu_i^2)}{E_i} \tag{4.2}$$

The next important step towards the determination of plastic properties of materials by indentation techniques is attributed to Meyer, who derived the following empirical relation,[37]

$$P = \frac{Ka^m}{D^{m-2}} \tag{4.3}$$

where m is the hardening factor, D is the indenter's diameter, a is the contact radius of the indentation, and K is a material constant. The above relation, however, ignored the sinking-in or piling-up of the material at the circumference of contact area. Norbury and Samuels, later on, defined a numerical constant, c, which was demonstrated to be invariable for a given material and depended only on the strain hardening exponent. It is given by the relation,[38]

$$c^2 = a^2/Dh \tag{4.4}$$

Hill, in 1945, showed that for ideal plastic materials,[39]

$$P_m = cY \tag{4.5}$$

where P_m is the mean resistive pressure or hardness of the material and Y is the yield stress. Tabor, in 1948, showed that the constant c has a value of 1.1 at the onset of plastic deformation and has a value of 3 in the fully plastic state. He also related the true plastic strain, ε_p, to the ratio of residual contact diameter, d, and indenter diameter, D, by the empirical relation,[40]

$$\varepsilon_p = 0.2d/D \tag{4.6}$$

Sneddon, in 1965, studied the relationship between load and penetration with a rigid punch of arbitrary profile and developed the equation,[41]

$$P = \frac{4\mu a}{1 - \nu}\, h \tag{4.7}$$

where a is the radius of the punch, μ is the shear modulus, and ν is Poisson's ratio. The above equation is especially valid for the indentation of elastic half-space by a flat, cylindrical punch where the contact area between the indenter and the specimen remains constant during the initial withdrawal of the indenter. King, later on, obtained an equation relating the elastic modulus of the specimen to the initial slope of the unloading curve by differentiating Equation 4.7,

$$dP/dh = \beta E_r \sqrt{A} \tag{4.8}$$

where A is the contact area of the indenter and β is a numerical constant whose value for a circular punch is one.[30]

The analysis of Oliver and Pharr showed that the load-displacement relationships for many simple punch geometries could conveniently be written as,[28,29]

$$P = \alpha h^m \tag{4.9}$$

where α and m are constants. Also, the unloading data can be approximated by the relationship,

$$P = A(h - h_o)^m \tag{4.10}$$

where A and m are constants and h_o is the final displacement after unloading. Suresh et al.,[37] using load-depth sensing spherical indentations, analyzed the fully plastic regime of the unloading curve and proposed an equation for calculating the value of yield point. It is given by,

$$\sigma_y = \frac{P}{3A}\left(\frac{0.002}{\varepsilon_r}\right)^n \tag{4.11}$$

where σ_y is the yield strength of the material, which corresponds to a plastic strain of 0.002, ε_r is the true characteristic strain, A is the true contact area at loading and n is the strain hardening exponent. The above equation is used to some extent to estimate the yield stress and strain hardening exponent of materials since it does not require a prior knowledge of material-related parameters.

4.2 FINITE ELEMENT SIMULATION OF GLASSES

Elastic-plastic simulation of the indentation process was performed using ANSYS version 7.0 software package. The material was assumed to be isotropic, homogenous and rate-independent and was modeled using VISCO106 linear 4-node elements. A rigid indenter-flexible substrate contact analysis was chosen. The indenter (target) and substrate (contact) were modeled using TARGE169 and CONTA172 elements respectively. The whole system with the indenter and substrate was axisymmetric with 1317 nodes and 1287 elements. Bilinear isotropic strain hardening behavior was assumed, which uses a Von Mises yield criterion coupled with a user-defined strain hardening curve and an associative flow rule. The solution uses Newton-Raphson iteration with a minimum of 20 substeps and a maximum of 2000 substeps. The number of substeps can be varied accordingly to vary the number of loading and unloading data points.

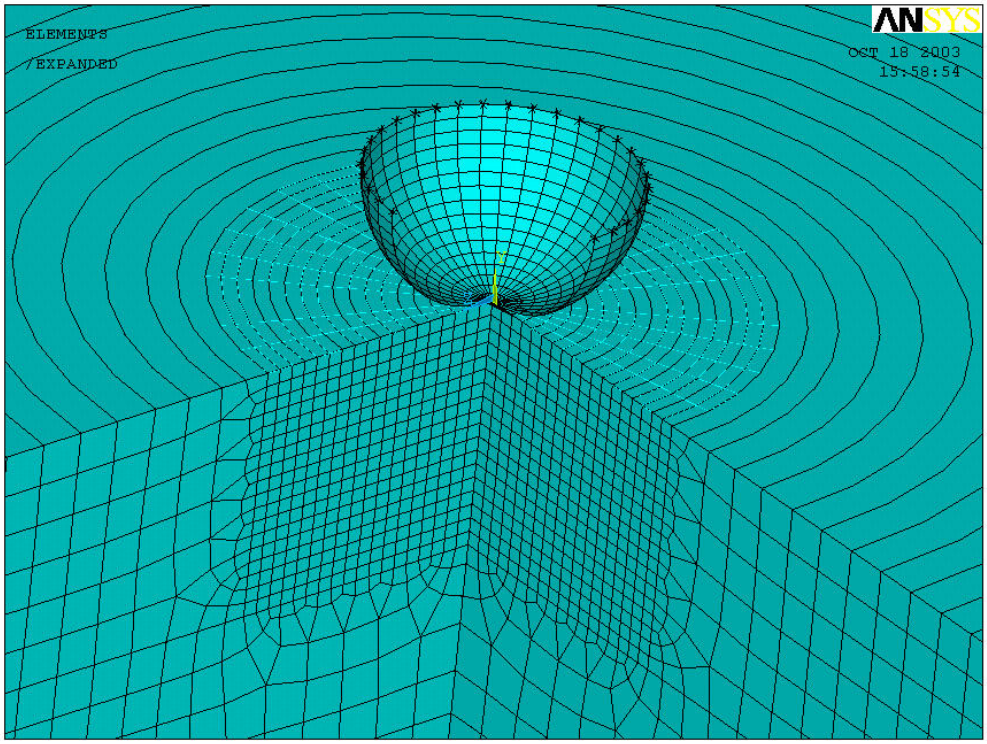

Figure 4.1. 3/4th slice of the expanded model with the indenter and substrate at zero contact.

A 3/4th 3D cyclic expansion of the model, with the rigid indenter just touching the substrate, is shown in Figure 4.1. The model was initially built with 228 nodes and analyzed. The size of the model and mesh were optimized until the dynamic indentation curves were smoothened. The radial and vertical dimensions of the body were 20 times the indentation depth, which made sure that the model approximated that of a semi-infinite body. Driving the target vertically through a pilot node by the application of a constant force, simulating the experimental conditions, made indentations. The target can also be driven to a constant penetration depth, with penetration depth values taken from experiments.

4.3 FEA CALCULATIONS AND COMPARISON WITH EXPERIMENTAL RESULTS

Elastic modulus, Poisson's ratio and an assumed yield stress are input to the analysis. Elastic modulus and Poisson's ratio were taken from prior investigators results through the equations,[11,17]

$$E\ (GPa) = 15.29\langle r\rangle - 21.68 \tag{4.12}$$

$$\nu = 0.5055 - 0.0919\langle r\rangle \tag{4.13}$$

The FEA simulation yielded load vs penetration curves from which both h_o/h_{max} and E (from the slope of the unloading curve) could be computed. Both the values were then compared with experimental data and a new yield stress input was made. Matching of E was more sensitive to the yield stress input. Iteration was stopped when E matched within ~1.5GPa (Figure 4.2). The FEA calculated values were generally higher most of the time. Matching of h_o/h_{max} allowed a good match between experimentally measured LBH or DBH and those calculated (Figure 4.3 for the 2mm ball indenter). The important point is that the local maximum observed in experimental DBH at $\langle r\rangle = 2.4$ for binary glasses is also observed in computed results. This indicates that glass of the coordination number 2.4 recovers to a lower final penetration depth according to both experimental and computed results.

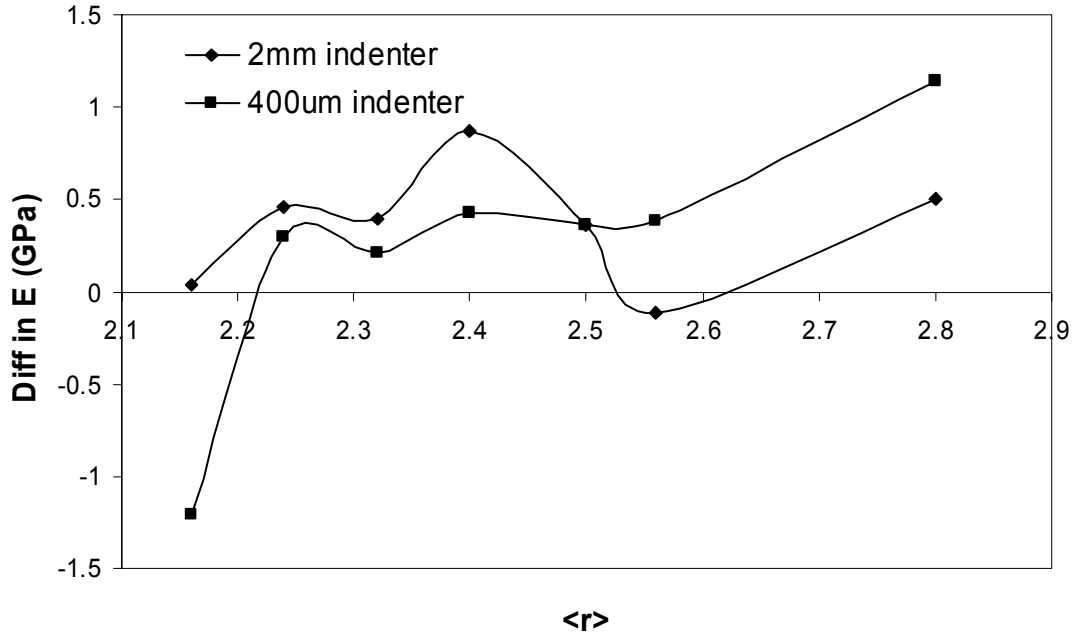

Figure 4.2. Difference between computed and experimental E values. A difference of zero indicates a perfect match while a positive value indicates that the computed value is higher than the experimental value.

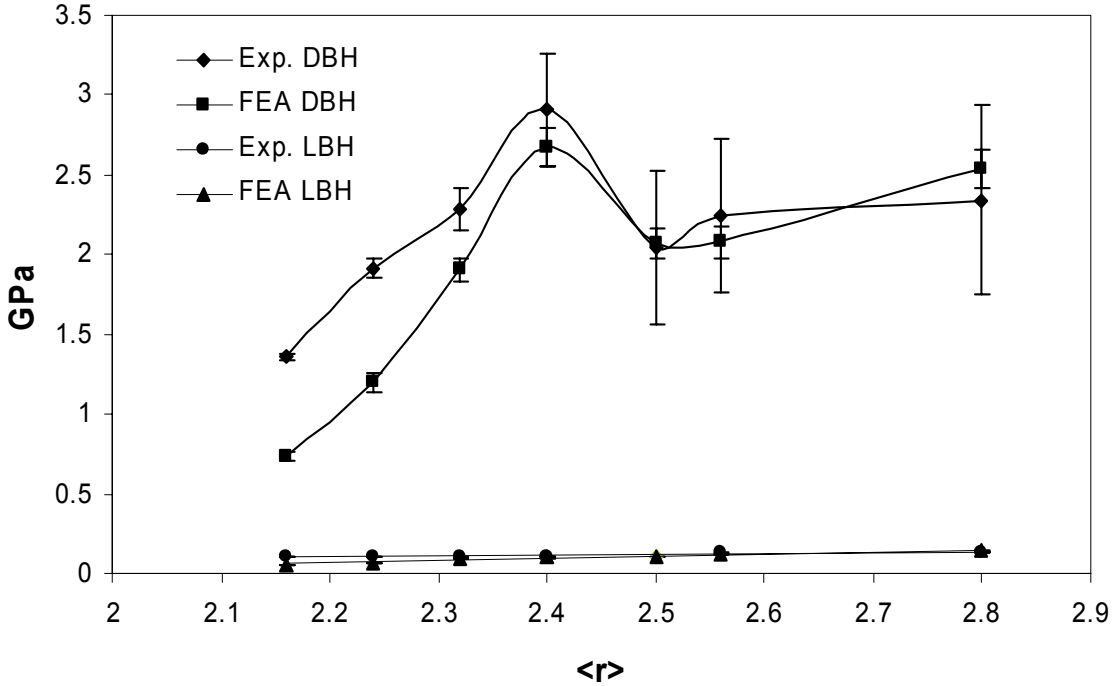

Figure 4.3. Comparison between computed and experimental LBH and DBH values obtained with a 2mm ball indenter.

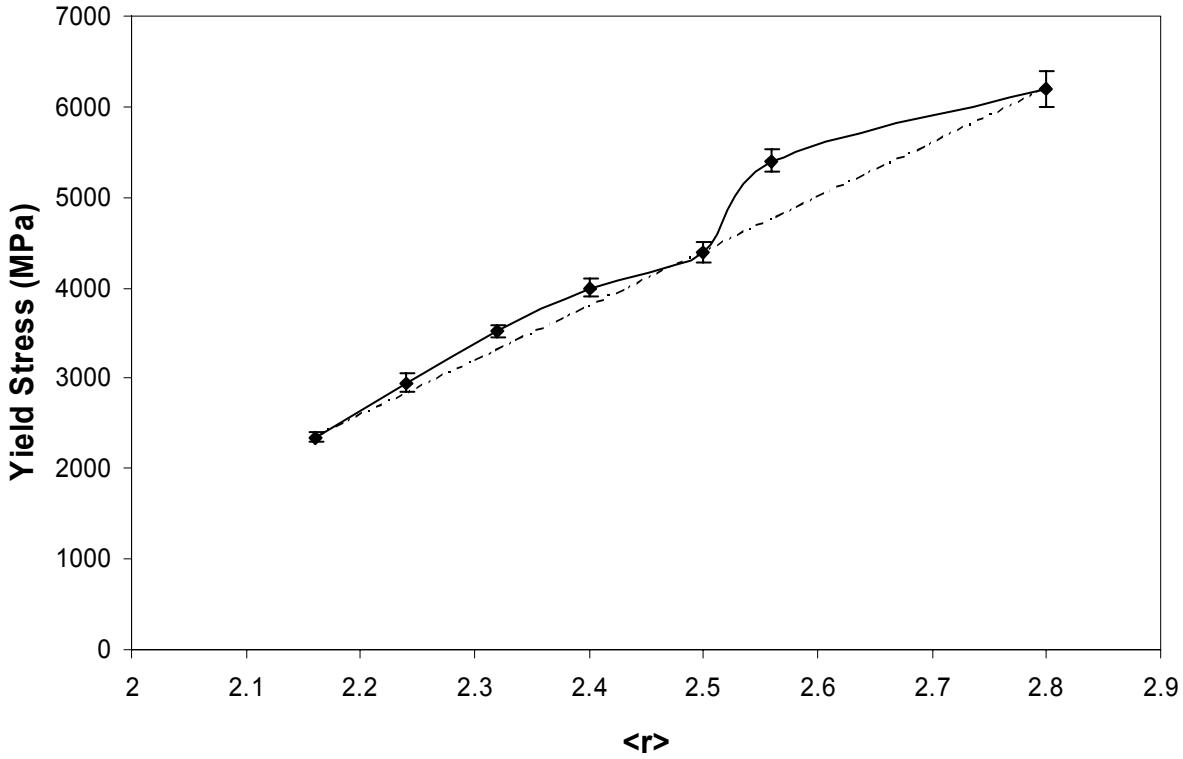

Figure 4.4. Computed yield stress as a function of <r> for the binary system. Apparent linearity is indicated by the dotted line.

Stresses and strains calculated from the finite element analysis are plotted as a function of <r> for the 400μm ball indenter in Figure 4.5 and Figure 4.6 respectively. Y-axis represents the direction of loading (lateral crack driving stress) whereas X- and Z-axes represent radial and median crack driving stresses respectively. It is noted that the stresses increase and strains decrease as <r> increases. This is due to increasing elastic modulus values with <r>. The lateral crack driving stress increases as the load increases, attains a maximum at the maximum load and starts to decrease as the load is retracted. However, the radial crack driving stress continues to increase even during unloading. The X-unloading stress remains almost constant throughout the composition range indicating no difference in cracking behavior between different glasses.

Figure 4.7 and Figure 4.8 show similar plots for stresses and strains as a function of <r> for 2mm ball indenter. Lateral crack driving stress and strain values observed with the 400μm ball indenter are almost twice than that observed with 2mm ball indenter. So, it can be concluded that the maximum stresses and strains decrease as the ball diameter increases.

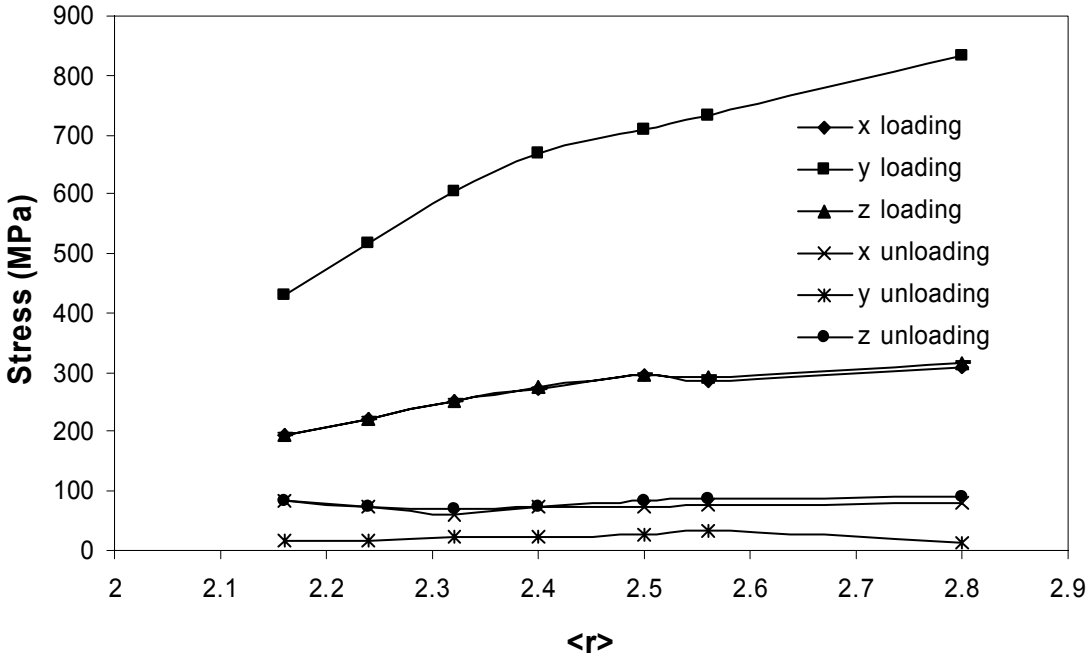

Figure 4.5. Radial, lateral and median (X, Y and Z) crack driving stresses as a function of <r> for the binary system obtained with the 400μm ball indenter.

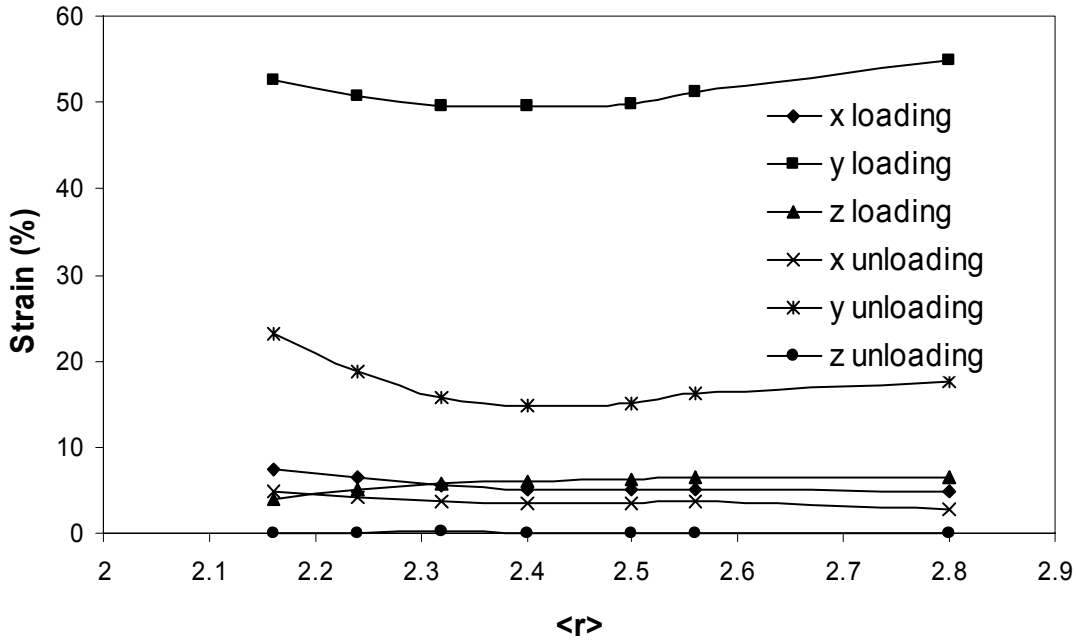

Figure 4.6. Radial, lateral and median (X, Y and Z) crack driving strains as a function of <r> for the binary system obtained with the 400μm ball indenter.

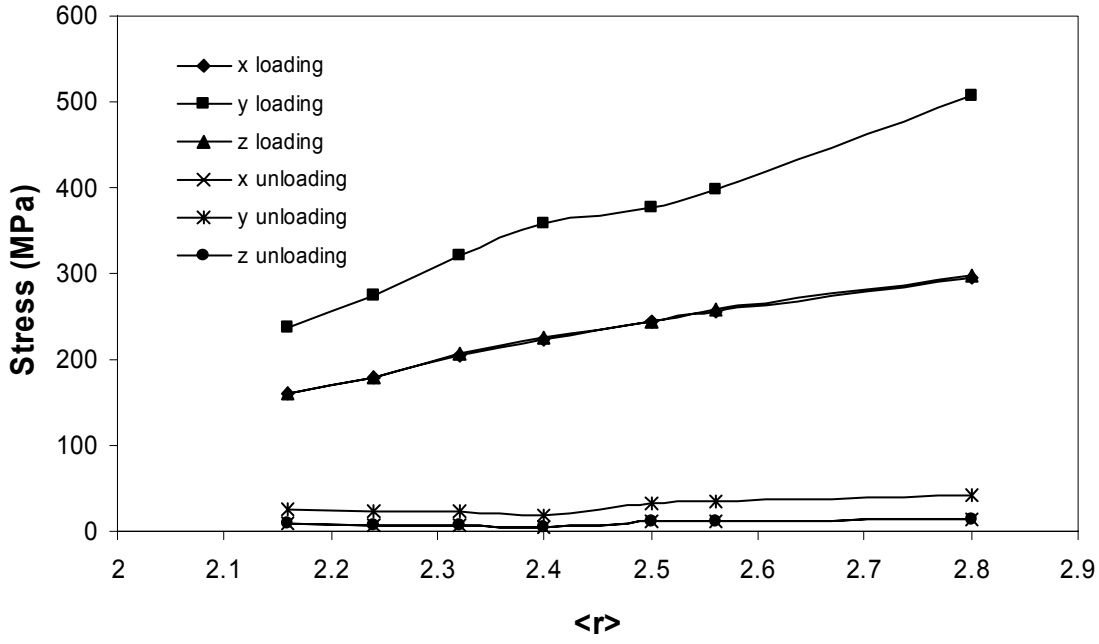

Figure 4.7. Similar plot showing stresses versus <r> for the 2mm ball indenter.

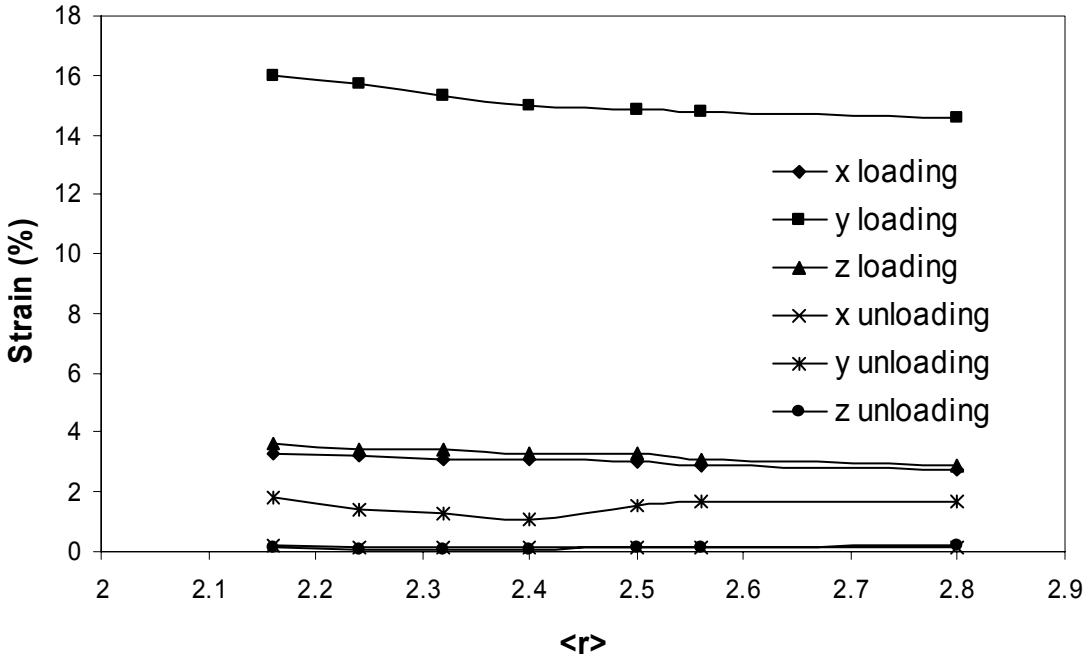

Figure 4.8. Similar plot showing strains versus <r> for the 2mm ball indenter.

The computed yield stress, plotted as a function of <r> for the Ge-Se binary system, is shown in Figure 4.4. Yield stress, in general, increases as the coordination number increases. This is due to the increase in the stress built-up rate with <r>. However, the plot does not seem to follow a linear trend. To be noted are the values of yield stress in the vicinity of <r> = 2.4 and <r> = 2.67. Those values seem to be slightly deviated from the linear trend observed for other glasses. The computed FEA results show that those small deviations in yield stress from apparent linearity may be sufficient to produce extrema in properties observed.

5 OVERALL DISCUSSION AND CONCLUSIONS

The theory of rigidity percolation may be used to explain the trends observed in Ge-Se binary glasses. It is not exactly known what happens when antimony is added to the binary system. One possibility is that antimony may increase the connectivity of the network thereby increasing the hardness or brittleness of the glass. This hypothesis is consistent with all the observations. If glasses of the compositions $Ge_{20}Se_{80}$ (<r> = 2.4) and $Ge_{12.5}Sb_{15}Se_{72.5}$ (<r> = 2.4) are compared, it is clear that twice as many 3-coordinated antimony atoms replace every 4-coordinated germanium atom. Since equal amount of selenium atoms are also taken out of the system, the connectivity of the ternary glass should be higher than that of the binary glass.

In the binary system, glasses below and above <r> = 2.4 showed significant cracking during static indentation measurements. Brittleness was found to approach a minimum and fracture toughness a maximum at <r> = 2.4. However, the radial crack driving stresses calculated from FEA do not show any difference in the cracking behavior between different glasses. If glasses of the coordination number 2.4 do not show any radial cracking on unloading, there should be a maximum observed in the radial crack driving stress at <r> = 2.4. Instead, the radial crack driving stress is relatively higher for the coordination number 2.8, which has the highest brittleness value in the system.

The various criteria for defining the preferred direction of crack propagation fall into two categories: energy methods and stress methods. Energy methods propose that the crack will propagate in the direction of the maximum energy release rate while the stress methods assume that the crack will propagate in the direction that maximizes the fracture.[42] According to energy methods, if $Ge_{20}Se_{80}$ glasses were to have higher fracture toughness values or higher preferential elastic recovery in the loading direction, lateral cracking should predominate. However, the values of lateral crack driving stress during unloading do not show any dip at that composition.

Poisson's ratio is a means to describe the relationship between the volume change and stress applied. Poisson's ratio decreases linearly with <r> for the binary system following the equation, $\nu = 0.5055 - 0.0919\langle r \rangle$, as determined by Sreeram and others.[11] If $\langle r \rangle = 0$, then $\nu \sim 0.5$, results in an ideally plastic or completely incompressible system, which, in turn, means that the material maintains constant volume regardless of the stress applied (zero elastic modulus or infinite bulk modulus).

Piling-up of the material around the indentation corners is directly proportional to the depth penetrated by the indenter; lower penetration depths giving lower pile-up heights. Also, higher elastic recovery of the material in the vertical direction during unloading results in lower plasticity created by the indenter, which, in turn, results in lower pile-up height around the indention corners. If the plastic deformation maintains constant volume during indentation, then the pile-up height observed would still be low. Since glasses of the coordination number 2.4 have the highest elastic recovery, the amount of plastically deformed material around the indentation corners would be low, giving rise to low pile-up heights. This can be observed using surface roughness (contact profilometer/laser interferometer) measurements. Furthermore, a smaller diameter ball indenter would penetrate deeper in to the material and hence would create higher pile-up heights around indention corners when compared to a larger diameter indenter.

The maximum observed in DBH and fracture toughness for $Ge_{20}Se_{80}$ may be attributed to the observed minimum in brittleness and it can be argued that the lack of radial cracking leaves more of the energy of indentation available for elastic recovery. However, brittleness is itself a ratio of hardness to fracture toughness. Yield stress, on the other hand, is an intrinsic property of a material and properties such as the fracture toughness can directly be correlated to it. Calculations from FEA also support this argument. Even though there is no difference seen in cracking behavior between different glasses, there are differences in the values of yield stress. Yield stress values for glasses of the composition $Ge_{20}Se_{80}$ are slightly deviated from the linear trend observed for other glasses, which may be sufficient to produce extrema in DBH.

The conclusions drawn from this work can be summarized as follows:

- Binary glasses show maximum elastic recovery, DBH, indentation toughness and minimum brittleness at <r> = 2.4.
- However, ternary glasses do not show any such trends.
- Examination of the energies of indentation as a function of the indenter diameter reveals that the elastically recovered energy increases with the indenter diameter. Additionally, the plasticity/elasticity ratio approaches a minimum at the composition $Ge_{20}Se_{80}$.
- The data computed from finite element calculations also show similar trends for LBH and DBH. Increasing elastic moduli cause stresses to increase with <r> for a given indenter ball diameter. Furthermore, maximum stresses are found to decrease with increasing indenter ball diameter.
- Computed yield stresses, when plotted against <r>, show small deviations from apparent linearity at <r> = 2.4. This may be sufficient to produce extrema in the properties observed.

6 FUTURE WORK

The term "coordination number" itself is a simple representation of the connectivity of the network and does not give a complete picture of the network structure. This is evident when the two glasses $Ge_{20}Se_{80}$ (<r> = 2.4) and $Ge_{12.5}Sb_{15}Se_{72.5}$ (<r> = 2.4) are compared; one showing the "magic trends" whereas the other does not. In order to have a complete understanding of the network structure, the bonding between individual atoms need to be studied. Molecular dynamic simulations of glasses would reveal the bonding between individual atoms, the percentage of bonding between particular pair of atoms and so on.

The surface roughness of the indented samples can be observed using contact profilometer or laser interferometer. Using these measurements, the amount of plastic pile-up around indentation corners of different glasses can be compared.

The cracking behavior of different glasses needs to be studied. The effect of formation of radial, median and lateral cracks during loading and unloading can be included in the model and hence the elastic recovery measurements can directly be correlated to it.

SEM and EDS analysis of etched samples would determine the presence of phase separation, which, in turn, can be used to establish the immiscibility and spinodal domes.

Finite element and molecular dynamic simulations can be used to study the response of atoms to indentations. The displacement of atoms due to indentations can in turn be used to calculate the bond energy in the localized area of indentation, which, in turn, would lead to a better understanding of the network.

REFERENCES

1. A.B. Seddon, "Chalcogenide Glasses: A Review of Their Preparation, Properties and Application," *J. Non-Cryst. Solids*, **184**, 44-50 (1995).

2. A.K. Varshneya, *Fundamentals of Inorganic Glasses*, Academic Press, Boston, MA, 1994.

3. J.P. Guin, T. Rouxel, and J.C. Sangleboeuf, "Hardness, Toughness and Scratchability of Germanium-Selenium Chalcogenide Glasses," *J. Am. Ceram. Soc.*, **85** [6] 1545-52 (2002).

4. K. Tanaka, "Layer Structures in Chalcogenide Glasses," *J. Non-Cryst. Solids,* **103**, 149-150 (1988).

5. J.C. Phillips, "Topology of Covalent Non-crystalline Solids I: Short-range Order in Chalcogenide Alloys," *J. Non-Cryst. Solids,* **34**, 153-81 (1979).

6. G.H. Dohler, R. Dandoloff, and H. Bilz, "A Topological-Dynamical Model of Amorphicity," *J. Non-Cryst. Solids,* **42**, 87-96 (1981).

7. J.C. Phillips, "Structural Principles of Amorphous and Glassy Semiconductors," *J. Non-Cryst. Solids,* **35-36**, 1157-65 (1980).

8. J.C. Phillips and M.F. Thorpe, "Constraint Theory, Vector Percolation and Glass Formation," *Solid State Commun.*, **53** [8] 699-702 (1985).

9. M.F. Thorpe, "Rigidity Percolation in Glassy Structures," *J. Non-Cryst. Solids,* **76**, 109-16 (1985).

10. K. Tanaka, "Structural Phase Transitions in Chalcogenide Glasses," *Phys. Rev. B: Condens. Matter*, **39** [2] 1270-9 (1989).

11. A.K. Varshneya, A.N. Sreeram, and D.R. Swiler, "A Review of the Average Coordination Number Concept in Multicomponent Chalcogenide Glass Systems," *Phys. Chem. Glasses*, **34** [5] 179-92 (1993).

12. A.N. Sreeram, A.K. Varshneya, and D.R. Swiler, "Microhardness and Indentation Toughness versus Average Coordination Number in Isostructural Chalcogenide Glass Systems," *J. Non-Cryst. Solids,* **130**, 225-35 (1991).

13. A.N. Sreeram, D.R. Swiler, and A.K. Varshneya, "Gibbs-DiMarzio Equation to Describe the Glass Transition Temperature Trends in Multicomponent Chalcogenide Glasses," *J. Non-Cryst. Solids,* **127**, 287-97 (1991).

14. A.N. Sreeram, A.K. Varshneya, and D.R. Swiler, "Molar Volume and Elastic Properties of Multicomponent Chalcogenide Glasses," *J. Non-Cryst. Solids,* **128**, 294-309 (1991).

15. K. Firstenberg, "Microhardness of Chalcogenide Glasses: Static and Dynamic Indentation Measurements"; M.S. Thesis, Alfred University, Alfred, NY, 1999.

16. D. Strange, "Micromechanical Properties of Glass in the Ge-Sb-Se System"; M.S. Thesis, Alfred University, Alfred, NY, 2001.

17. U. Senapati, "Physical Property Changes Associated with Glass Transition in Chalcogenide Glasses"; Ph. D. Thesis, Alfred University, Alfred, NY, 1997.

18. U. Senapati and A.K. Varshneya, "Configurational Arrangements in Chalcogenide Glasses: A New Perspective on Phillips' Constraint Theory," *J. Non-Cryst. Solids,* **185**, 289-96 (1995).

19. U. Senapati and A.K. Varshneya, "Viscosity of Chalcogenide Glass-forming Liquids: An Anomaly in the 'Strong' and 'Fragile' Classification," *J. Non-Cryst. Solids,* **197**, 210-18 (1996).

20. C.A. Angell, "Spectroscopy Simulation and Scattering, and the Medium Range Order Problem in Glass," *J. Non-Cryst. Solids,* **73**, 1-17 (1985).

21. C.A. Angell, "Perspective on the Glass Transition," *J. Non-Cryst. Solids,* **49**, [8] 863-871 1988.

22. C.A. Angell, "Relaxation in Liquids, Polymers and Plastic Crystals – Strong/Fragile Patterns and Problems," *J. Non-Cryst. Solids,* **131-133**, 13-31 (1991).

23. Xingwei Feng, W.J. Bresser, Min Zhang, B. Goodman, and P. Boolchand, "Role of Network Connectivity on the Elastic, Plastic and Thermal Behavior of Covalent Glasses," *J. Non-Cryst. Solids,* **222**, 137-143 (1997).

24. S. Chakravarty, D.G. Georgiev, and P. Boolchand, "Aging, Fragility and Reversibility Windows in Bulk Alloy Glasses," Department of Electrical & Computer Engineering and Computer Science, University of Cincinnati, Cincinnati, OH, (in press).

25. B. Bowden, "Recording Microspherical Indentation of Glass in the Ge-Se System"; B.S. Thesis, Alfred University, Alfred, NY, 2002.

26. A.M. Reitter, A.N. Sreeram, A.K. Varshneya, and D.R. Swiler, "Modified Preparation Procedure for Laboratory Melting of Multicomponent Chalcogenide Glasses," *J. Non-Cryst. Solids,* **139**, 121-128 (1992).

27. W. Mason, P.F. Johnson, and J.R. Varner, "Data from Recording Microhardness Testers," *J. Mater. Res.*, **7** [11] 3112-19 (1992).

28. G.M. Pharr, W.C. Oliver, and F.R. Brotzen, "On the Generality of the Relationship among Contact Stiffness, Contact Area and Elastic Modulus during Indentation," *J. Mater. Res.,* **7** [3] 613-16 (1992).

29. W.C. Oliver and G.M. Pharr, "An Improved Technique for Determining Hardness and Elastic Modulus Using Load and Displacement Sensing Indentation Experiments," *J. Mater. Res.,* **7** [6] 1564-80 (1992).

30. R.B. King, "Elastic Analysis of Some Punch Problems for a Layered Medium," *Int. J. Solids Structures*, **23** [12] 1657-64, (1994).

31. J. Malzbender, G. de With, and J.M.J. den Toonder, "Determination of the Elastic Modulus and Hardness of Sol-Gel Coatings on Glass: Influence of Indenter Geometry," *Thin Solid Films*, **372** [1-2] 134-43 (2000).

32. U. Senapati, K. Firstenberg, and A.K. Varshneya, "Structure-Property Inter-relations in Chalcogenide Glasses and Their Practical Implications," *J. Non-Cryst. Solids,* **222**, 153-59 (1997).

33. G.R. Anstis, P. Chantikul, B.R. Lawn, and D.B. Marshall, "A Critical Evaluation of Indentation Techniques for Measuring Fracture Toughness: I, Direct Crack Measurements," *J. Am. Ceram. Soc.,* **64** [9] 533-38 (1981).

34. B.R. Lawn and D.B. Marshall, "Hardness, Toughness, and Brittleness: An Indentation Analysis," *J. Am. Ceram. Soc.,* **62** [7-8] 347-50 (1979).

35. J. Sehgal and S. Ito, "Brittleness of Glass," *J. Non-Cryst. Solids,* **253**, 126-32 (1999).

36. K.L. Johnson, *Contact Mechanics*; Ch. 5. Cambridge University Press, Cambridge, UK, 1985.

37. J. Alcala, A.E. Giannakopoulos, and S. Suresh, "Continuous Measurements of Load-Penetration Curves with Spherical Microindenters and the Estimation of Mechanical Properties," *J. Mater. Res.,* **13** [5] 1390-1400 (1992).

38. A.L. Norbury and T. Samuel, "The Recovery and Sinking-in or Piling-up of Material in the Brinell Test, and the Effects of these Factors on the Correlation of the Brinell with Certain Other Hardness Tests," *J. Iron Steel Inst.* **117**, 673-87 (1928).

39. R. Hill, *The Mathematical Theory of Plasticity*; pp. 254-61. Clarendon Press, Oxford, England, 1950.

40. D. Tabor, *The Hardness of Metals*, Clarendon Press, Oxford, England, 1951.

41. I.N. Sneddon, "The relation between load and penetration in the axisymmetric boussinesq problem for a punch of arbitrary profile," *Int. J. Eng. Sci.*, **3**, 47-57 (1965).

42. M.B. Bush, "Simulation of Contact-induced Fracture," *Eng. Anal. Boundary Elem.*, **23**, 59-66 (1999).